The Yarkovsky and YORP Effects: Implications for Asteroid Dynamics

William F. Bottke, Jr.,[1] David Vokrouhlický,[2] David P. Rubincam,[3] and David Nesvorný[1]

[1]Southwest Research Institute, Boulder, Colorado 80302; email: bottke@boulder.swri.edu

[2]Institute of Astronomy, Charles University, 18000 Prague 8, Czech Republic

[3]NASA Goddard Space Flight Center, Greenbelt, Maryland 20771

Annu. Rev. Earth Planet. Sci. 2006. 34:157–91

First published online as a Review in Advance on January 16, 2006

The *Annual Review of Earth and Planetary Science* is online at earth.annualreviews.org

doi: 10.1146/annurev.earth.34.031405.125154

0084-6597/06/0530-0157$20.00

Key Words

asteroids, meteorites, asteroids-dynamics, celestial mechanics, nongravitational forces

Abstract

The Yarkovsky and YORP (Yarkovsky-O'Keefe-Radzievskii-Paddack) effects are thermal radiation forces and torques that cause small objects to undergo semimajor axis drift and spin vector modifications, respectively, as a function of their spin, orbit, and material properties. These mechanisms help to (*a*) deliver asteroids (and meteoroids) with diameter $D < 40$ km from their source locations in the main belt to chaotic resonance zones capable of transporting this material to Earth-crossing orbits; (*b*) disperse asteroid families, with drifting bodies jumping or becoming trapped in mean-motion and secular resonances within the main belt; (*c*) modify the rotation rates and obliquities of $D < 40$ km asteroids; and (*d*) allow asteroids to enter into spin-orbit resonances, which affect the evolution of their spin vectors and feedback into the Yarkovsky-driven semimajor axis evolution. Accordingly, we suggest that nongravitational forces should now be considered as important as collisions and gravitational perturbations to our overall understanding of asteroid evolution.

1. INTRODUCTION

NEO: near-Earth object
CM: classical model

The motions of celestial bodies are usually considered to be the sole domain of gravity. For this reason, the conventional wisdom over the past several decades has been that collisions and gravitational forces are the primary mechanisms governing the evolution of asteroids and their fragments. Using these processes, it is possible to construct, with some success, an approximate history of how the main belt and inner Solar System asteroid populations have changed over the past several billion years. To set the stage for our discussion of how nongravitational forces affect asteroids, we summarize below the main points of this so-called classical asteroid evolution model (see also Bottke et al. 2002b).

The largest reservoir of asteroids in the inner Solar System is the main belt, located between 2.0–3.3 AU (i.e., between the orbits of Mars and Jupiter). It currently holds ~1 million objects with diameter $D > 1$ km (e.g., Bottke et al. 2005a,b). It is believed that this population is the primary source for the near-Earth object (NEO) population, which includes both asteroids and some active/extinct comets that have perihelion distances $q \leq 1.3$ AU and aphelion distances $Q \geq 0.983$ AU. The meteoroids and larger objects that strike the Earth and Moon over time come from this population. There are currently ~1000 NEOs with $D > 1$ km and semimajor axis $a < 7.4$ AU (Bottke et al. 2002b, Stuart & Binzel 2004). Numerical simulations indicate that the mean dynamical lifetimes of the NEOs are several millions of years (Gladman et al. 1997), although the distribution is bimodal (Bottke et al. 2002b). Only about 1% of the NEOs end up as Earth impactors (Gladman et al. 1997, Morbidelli & Gladman 1998); nearly all the rest impact the Sun or are ejected from the inner Solar System via a close encounter with Jupiter (Farinella et al. 1994, Gladman et al. 1997). Interestingly, the nearly constant crater production rates observed on the lunar maria indicate the NEO population has been in steady state (within a factor of 2 or so) over the last 3 Gy (Grieve & Shoemaker 1994; McEwen et al. 1997; Bottke et al. 2005a,b). This means that the mechanisms resupplying the NEO population are likely to be dominated by continuous processes rather than rare events.

According to the classical model (CM) of asteroid and meteorite delivery, where collisions and gravitational perturbations dominate evolutionary processes, how does the main belt resupply the NEO population? We know that asteroids, whose orbits intersect one another in the main belt, sporadically collide with one another at high velocities (~5 km s^{-1}; Bottke et al. 1994). These events result in cratering and fragmentation, with the collisional physics determining the orbits, spin states, shapes, and internal structures of the surviving bodies. The largest impact events are believed to produce the observed asteroid families, clusters of fragments having similar semimajor axis a, eccentricity e, and inclination i values. These orbital parameters, when used to infer the ejection velocities of the family members, indicate that many multikilometer objects were launched away from the impact site at ~several 100 m s^{-1} (Zappalà et al. 1996). Accordingly, asteroid ejecta, if thrown with just the right trajectory and velocity, could be injected into the powerful or diffusive resonance zones produced by the gravitational perturbations of the planets (Farinella et al. 1993). Numerical studies have shown that test objects in such resonance regions frequently have

their eccentricities pumped up to Mars-crossing or even NEO orbits (e.g., Wisdom 1983). Once on these orbits, asteroids have their dynamical evolution dominated by resonances and gravitational close encounters with the planets. Thus, to keep the NEO population in steady state, we need catastrophic collisions to occur frequently and within the range of resonances that can efficiently deliver the material to the inner Solar System.

CRE: cosmic-ray exposure

The CM of asteroid and meteorite delivery has helped us glean numerous insights into how individual asteroids as well as asteroid populations have evolved with time. Nevertheless, it makes several predictions that are inconsistent with observations. Several examples are given below.

CM Prediction 1: Most of the meteoroids delivered to Earth are directly injected into chaotic resonances. Because the dynamical lifetime of bodies placed in such powerful resonances are generally a few million years or less (Gladman et al. 1997), we should find an abundance of meteorites with short cosmic-ray exposure (CRE) ages (i.e., only a few million years) and a paucity of long-lived meteorites. Recall that CRE ages measure the length of time a body spends between its final reduction in size by impact, which places its entire interior within a few meters of the radiation environment, and delivery to Earth.

Observation 1: Most stony meteorites have CRE ages between ~10–100 My, while iron meteorites have CRE ages between ~ 0.1–1 Gy (e.g., Eugster 2003). Relatively few meteorites are found to have CRE ages shorter than a few million years. In general, CRE ages are comparable to, or longer than, the average dynamical lifetime of NEOs.

CM Prediction 2: There are roughly 5000–6000 kilometer-sized asteroids in the Mars-crossing and NEO populations (Bottke et al. 2002a). These bodies have a wide range of taxonomic types (e.g., Binzel et al. 2004). To keep this population in steady state, disruption events among large, spectrally diverse asteroids must be frequent, particularly because these are the only events capable of injecting kilometer-sized fragments into suitable resonant "escape hatches." Moreover, many longer-lived asteroids come from the inner and central main belt (Bottke et al. 2002b), such that we expect these regions to contain numerous asteroid families produced by recent breakup events. Finally, because the planet-crossing asteroids are "fresh ejecta," they should have a size-frequency distribution that has a steep power-law index.

Observation 2: Few recently produced asteroid families can be found in the inner and central main belt (Nesvorný et al. 2002a, 2003). Most potential parent asteroids for the kilometer-sized inner Solar System asteroids reside in dynamically stable regions far from resonant escape hatches (Nesvorný et al. 2002a). Modeling results including these constraints suggest that the direct injection of asteroid fragments into resonances is too inefficient to keep the inner Solar System asteroid population in steady state (Zappalà et al. 2002). In addition, the size-frequency distribution of kilometer-sized NEOs is shallower than one would expect from a population dominated by fresh ejecta (Morbidelli & Vokrouhlický 2003, Stuart & Binzel 2004, Bottke et al. 2005b, McEwen et al. 2005).

YORP: Yarkovsky-O'Keefe-Radzievskii-Paddack

CM Prediction 3: Studies of asteroid families suggest that many large fragments are ejected from the impact site at high velocities (~several 100 m s^{-1}), with the smallest fragments traveling the furthest from the cluster-center (Cellino et al. 1999).
Observation 3: The peak velocities of size-velocity distributions derived from numerical hydrocode results of asteroid collisions (Michel et al. 2001), as well as recent asteroid disruption events (e.g., <10 My for Karin and Veritas; Nesvorný et al. 2002a, 2003), are much lower ($\lesssim$100 m s^{-1}) than those inferred from the orbital positions of more evolved asteroid family members.
CM Prediction 4: Asteroid collisions should produce a wide range of asteroid spin rates. To zeroth order, we would expect the spin rates for large and small asteroids to follow a Maxwellian frequency distribution (e.g., Binzel et al. 1989, Davis et al. 1989).
Observation 4: The distribution of spin rates among observed small asteroids ($D <$ 10 km) contains an excess number of fast rotators and very slow rotators when this data is fit to Maxwellian distribution (Pravec & Harris 2000, Pravec et al. 2002).

We believe these mismatches are best explained as a consequence of nongravitational forces affecting asteroid evolution. Specifically, the CM does not include the so-called Yarkovsky effect, a thermal thrust produced when small bodies orbiting the Sun absorb sunlight, heat up, and reradiate the thermal energy after a short delay produced by thermal inertia. This emission, while tiny, produces a force that can lead to secular changes in the object's semimajor axis, causing $D = 0.1$ m to ~40 km objects to spiral inward or outward at different rates as a function of their spin, orbit, and material properties. This same force produces a torque called the Yarkovsky-O'Keefe-Radzievskii-Paddack (YORP) effect, which is also capable of modifying the spin rates and axis orientations of asteroids. These thermal forces, which have been mostly ignored over the past several decades, are capable of resolving the problems described above. Accordingly, we believe the CM should now be revised to include nongravitational forces as a third important mechanism, in addition to gravity and collisions, affecting asteroid evolution.

2. INTRODUCTION TO THE YARKOVSKY EFFECT

Ivan Osipovich Yarkovsky (1844–1902), a civil engineer who worked on scientific problems in his spare time, first proposed the effect that now bears his name (Neiman et al. 1965, Beekman 2005). Writing in a pamphlet around the year 1900, Yarkovsky noted that the diurnal heating of a rotating object in space would cause it to experience a force that, while tiny, could lead to large secular effects in the orbits of small bodies, especially meteoroids and small asteroids (Öpik 1951). Yarkovsky's effect is a radiation force, and is the photonic equivalent of Whipple's (1950) rocket effect.

Yarkovsky's remarkable insight would have been consigned to oblivion had it not been for the brilliant Estonian astronomer Ernst J. Öpik (1893–1985), who read Yarkovsky's pamphlet sometime around 1909. Decades later Öpik, recalling the pamphlet from memory, discussed the possible importance of the Yarkovsky effect for moving meteoroids about the Solar System (Öpik 1951). (Curiously, Öpik's (1976) book, which continues the theme of his 1951 paper, makes no mention of Yarkovsky).

Following Öpik and before its current flowering, research on Yarkovsky-type effects was pursued in Russia by Radzievskii (1952, 1954) and Katasev & Kulikova (1980); in the United States by Paddack (1969, 1973), Paddack & Rhee (1975), Peterson (1976), O'Keefe (1976), Slabinski (1977), Dohnanyi (1978), and Burns et al. (1979); and in Australia by Olsson-Steel (1986, 1987). Additional history on the Yarkovsky effect can be found in Hartmann et al. (1999).

2.1. Description of Diurnal Component

The basic idea behind Yarkovsky's diurnal effect is shown in **Figure 1*a***, which shows a spherical meteoroid in a circular orbit about the Sun. For simplicity, the meteoroid's spin axis is taken to be normal to the orbital plane, so that the Sun always stands on its equator. Insolation heats up the sunward side, with the heat ultimately reradiated into space by the meteoroid (typically in the infrared part of the spectrum, unless the meteoroid is very close to the Sun). An infrared photon carries away momentum

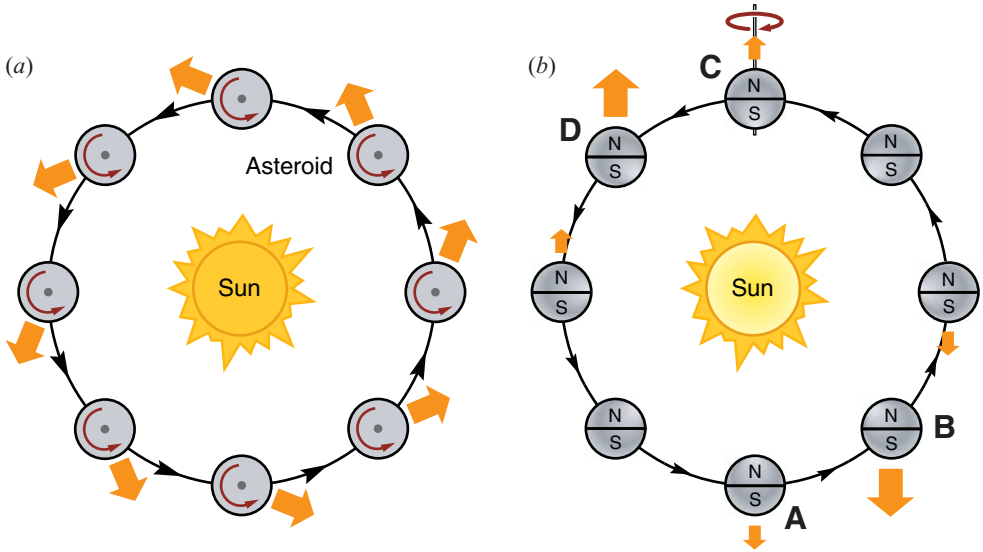

Figure 1

(*a*) The diurnal Yarkovsky effect, with the asteroid's spin axis perpendicular to the orbital plane. A fraction of the solar insolation is absorbed only to later be radiated away, yielding a net thermal force in the direction of the wide arrows. Because thermal reradiation in this example is concentrated at about 2 PM on the spinning asteroid, the radiation recoil force is always oriented at about 2 AM. Thus, the along-track component causes the object to spiral outward. Retrograde rotation would cause the orbit to spiral inward. (*b*) The seasonal Yarkovsky effect, with the asteroid's spin axis in the orbital plane. Seasonal heating and cooling of the "northern" and "southern" hemispheres give rise to a thermal force, which lies along the spin axis. The strength of the reradiation force varies along the orbit as a result of thermal inertia; even though the maximum sunlight on each hemisphere occurs as A and C, the maximum resultant radiative forces are applied to the body at B and D. The net effect over one revolution always causes the object to spiral inward.

when it leaves the meteoroid according to the relation $p = E/c$, where p is the photon's momentum, E its energy, and c is the speed of light. Because more energy and therefore more momentum departs from the hotter part of the meteoroid than the colder, the meteoroid feels a net kick in the direction away from the hotter part.

If the meteoroid had no thermal inertia, then the temperature distribution would be symmetrical about the subsolar point and the meteoroid would experience a net force radially outward from the Sun. The only consequence of this force would be to weaken the Sun's grip on the meteoroid. However, all bodies have thermal inertia, which causes a delay, so that the hottest part of the meteoroid is its afternoon side rather than the subsolar point. This is similar to Earth, where afternoon rather than noon is the warmest time of day. As a result, the force on the meteoroid has not only a component which is radially outward from the Sun but also has an along-track component.

This along-track component causes a secular increase in the semimajor axis (and, to a lesser degree, eccentricity) for the prograde sense of rotation shown in the figure, so that over time the tiny Yarkovsky force can profoundly change the orbit. The sign of the diurnal Yarkovsky effect depends on the sense of rotation. If the meteoroid shown in **Figure 1*a*** rotated in the retrograde sense, the orbit would shrink instead of expand, whereas if the rotation axis was in the orbital plane, the diurnal Yarkovsky would be shut off entirely. The magnitude of the diurnal effect also depends on how close a body is to the Sun, the tilt of the body's spin axis with respect to the orbital plane, and the body's physical characteristics (i.e., the size of the body, its shape and thermal properties, and how fast it is rotating). The interplay of these factors means that there is an optimal size for maximizing the diurnal Yarkovsky effect for a given rotation speed and thermal structure. A very large object would have a poor area-to-mass ratio (e.g., the effect is negligible on a large body like Earth). On the other hand, the smaller the body, the better the area-to-mass ratio, but at some point the radius becomes so small that the thermal wave penetrates all the way across the body, lessening the temperature differences between the night and day sides and weakening the effect (e.g., a slowly rotating dust particle). For rotation periods believed to be typical in the Solar System, roughly $P \sim 5$ (D/2), where D is the diameter in meters and P is in seconds, optimal sizes for the Yarkovsky effect range from centimeters to meters. Objects having zero or infinitely fast rotation rates experience no diurnal Yarkovsky force.

2.2. Description of Seasonal Component

Nearly a century after Yarkovsky wrote his pamphlet, a second variant of the Yarkovsky effect emerged. While searching for the cause of the secular decay of the orbit of the LAGEOS satellite, it was realized that there had to be a seasonal effect (Rubincam 1987, 1988, 1990) in addition to Yarkovsky's original diurnal effect. The seasonal effect applies not just to Earth satellites like LAGEOS but also to objects orbiting the Sun.

The seasonal Yarkovsky effect is illustrated in **Figure 1*b***. As in **Figure 1*a***, a spherical meteoroid is assumed to be in a circular orbit about the Sun, but in this

case the spin axis lies in the orbital plane. It is the component of force lying along the spin axis that gives rise to the seasonal effect. When the meteoroid is at A (bottom of the figure) the Sun shines most strongly on its northern hemisphere. As with the diurnal effect, there is a delay due to thermal inertia, so that the northern hemisphere is hottest at B. Likewise, the Sun shines most strongly on the southern hemisphere at C but this hemisphere becomes hottest at D. Although the radiation reaction force is symmetrical in **Figure 1*b***, the changing velocity vector assures that the net effect shrinks the orbit. For a body without thermal inertia, however, the along-track force averages to zero when integrated over one revolution about the Sun.

For small orbital eccentricities, the average along-track force always opposes the motion of the meteoroid. Hence in the small eccentricity regime the seasonal force always acts like drag and causes orbital decay; for this reason the seasonal Yarkovsky effect was originally dubbed "thermal drag" (Rubincam 1987). Unlike the diurnal Yarkovsky effect, the seasonal Yarkovsky effect is independent of the sense of rotation of the meteoroid; reversing its spin does not change the effect's sign. Moreover, the relevant timescale for the seasonal effect is the meteoroid's orbital period rather than the usually much quicker rotational period involved in the diurnal effect.

The seasonal effect does depend on the body's proximity to the Sun and on the tilt of the spin axis with respect to the orbit; it vanishes when the spin axis is normal to the orbital plane. As in the diurnal case, there is an optimum size for maximizing the effect. For basaltic bodies on circular orbits in the inner main belt, $D \sim 10$ m objects would experience the greatest effects (Farinella et al. 1998, Rubincam 1998). The seasonal Yarkovsky force also affects the other orbital elements in addition to the semimajor axis. For small eccentricities it tends to circularize the orbit, as atmospheric drag does (Rubincam 1995, 1998; Vokrouhlický & Farinella 1998, 1999).

3. THEORY OF THE YARKOVSKY EFFECT

The Yarkovsky force computation naturally splits into two parts: (*a*) determination of the surface temperature distribution, and (*b*) evaluation of the thermal radiation recoil force (or torque if desired). Mathematically similar derivations of this solution can be found in several modern references (Rubincam 1995, 1998; Vokrouhlický 1998a,b, 1999; Vokrouhlický & Farinella 1999; Bottke et al. 2000b). In this section, we follow the formalism of Vokrouhlický (2001).

To compute the surface temperature on a body, we use the heat diffusion equations for energy flows inside the body:

$$\nabla \cdot (K \nabla T) = \rho C_p \frac{\partial T}{\partial t}, \tag{1}$$

or across its surface:

$$(K \nabla T \cdot \mathbf{n}_\perp) + \epsilon \sigma T^4 = \alpha \mathcal{E}, \tag{2}$$

the latter which appears as a boundary condition for the temperature (T) determination. The parameter K is the thermal conductivity, C_p is the specific heat at constant pressure, ρ is the material density, ϵ is the surface thermal emissivity, σ is the Stefan-Botzmann constant, and $\alpha = 1 - A$, with A being the Bond albedo. Equation 2

refers to a surface element with an external normal vector $\mathbf{n}_\perp$, whereas $\mathcal{E}$ is the flux of solar radiation through this element. Once the insolation function $\mathcal{E}$ for the surface elements is specified (which requires knowledge of the body's shape and its rotation state) and material parameters (K, C_p, ρ) are known, Equations 1 and 2 can be solved numerically.

At this point, it is useful to scale size and time to keep the number of parameters in our mathematical formulation as low as possible. For example, dimensional analysis shows that, for a given Fourier term with frequency ν in the decomposition of the insolation function $\mathcal{E}$, the problem involves two fundamental parameters: (*a*) the penetration depth of the thermal wave $\ell_\nu = \sqrt{K/\rho C_p \nu}$, and (*b*) the thermal parameter $\Theta_\nu = \sqrt{K\rho C_p \nu}/(\epsilon\sigma T_\star^3)$. Here $T_\star$ is the subsolar temperature defined by $\epsilon\sigma T_\star^4 = \alpha\mathcal{E}_\star$, with $\mathcal{E}_\star$ being the solar radiation flux at the distance of the body. The thermal parameter Θ_ν is a measure of the relaxation between the absorption and reemission at frequency ν. Thus, as Θ_ν grows smaller, the difference between the absorption and reemission grows smaller as well.

Solving for the temperature T, we can proceed to compute the recoil force (or torque) due to the thermal radiation (i.e., the Yarkovsky force). Assuming isotropic (Lambert) emission, the corresponding force per unit of mass is given by (Spitale & Greenberg 2001, Bottke et al. 2002a):

$$d\mathbf{f} = -\frac{2}{3}\frac{\epsilon\sigma}{mc}T^4\mathbf{n}_\perp dS(u,v), \qquad \mathbf{f} = \int_S d\mathbf{f}, \tag{3}$$

where the integration is to be performed over the whole surface parametrized by a system of coordinates u and v (such as the longitude and latitude in the spherical case), m is mass of the body and c the light velocity.

Adopting a local coordinate system with the z-axis aligned with the body's spin axis and the xy-axes in its equatorial plane, we can divide the Yarkovsky force into two variants: (*a*) the out-of-spin components (f_x,f_y) that depend primarily on the rotation frequency ω, and (*b*) the spin-aligned component f_z that depends only on the mean motion n. The former Yarkovsky-acceleration components are thus called diurnal, while the later is called seasonal (and they correspond to the qualitative concepts discussed in Section 2).

Yarkovsky accelerations primarily change a body's semimajor axis a. Because the perturbation is usually small, we average the variation in a over one revolution. Assuming a spherical body with radius R, and neglecting eccentricity e, the averaged diurnal and seasonal perturbations on da/dt are

$$\left(\frac{da}{dt}\right)_{\text{diurnal}} = -\frac{8\alpha}{9}\frac{\Phi}{n}F_\omega(R',\Theta)\cos\gamma + \mathcal{O}(e), \tag{4}$$

$$\left(\frac{da}{dt}\right)_{\text{seasonal}} = \frac{4\alpha}{9}\frac{\Phi}{n}F_n(R',\Theta)\sin^2\gamma + \mathcal{O}(e). \tag{5}$$

The total da/dt rate is the superposition of the two variants. The albedo-factor α in Equations 4 and 5 is close to that in Equation 2 (Vokrouhlický & Bottke 2001), $\Phi = \pi R^2\mathcal{E}_0/(mc)$ is the usual radiation pressure coefficient, and γ is obliquity of the spin axis. The function $F_\nu(R',\Theta)$ depends on the radius of the body R, scaled by the

penetration depth ℓ_ν of the thermal wave ($R' = R/\ell_\nu$), and the thermal parameter Θ_ν, both corresponding to the frequency ν.

For the diurnal effect, $\nu = \omega$, whereas for the seasonal effect, $\nu = n$. Note that apart from the different frequency, F is the same in Equations 4 and 5. The explicit form of F-function may be found in the literature (e.g., Vokrouhlický 1998a, 1999). Here, we restrict ourselves to mention its dependence on the thermal parameter:

$$F_\nu(R', \Theta) = -\frac{\kappa_1(R')\Theta_\nu}{1 + 2\kappa_2(R')\Theta_\nu + \kappa_3(R')\Theta_\nu^2}, \tag{6}$$

with κ_1, κ_2, and κ_3 analytic functions of R'. The frequency-index of F reminds us that both the scaling factor ℓ_ν of R and the thermal parameter Θ_ν depend on a given frequency. This parameter is the principal difference between the diurnal and seasonal Yarkovsky effects.

The da/dt rates listed above allow us to predict how the Yarkovsky perturbations change as a function of various parameters:

- Obliquity and rotation dependence: Because the F-functions are always negative (i.e., thermal reemission lags behind the absorption), the seasonal Yarkovsky effect always produces a net decrease in a. The seasonal effect is maximum at $\gamma = 90^\circ$ obliquity and zero at $\gamma = 0^\circ$ (or 180°) obliquity. On the other hand, the diurnal effect may lead to both a net increase in a (for $\gamma < 90^\circ$) or a net decrease in a (for $\gamma > 90^\circ$). The effect is maximum at 0° (or 180°) obliquity and zero for 90° obliquity. The diurnal Yarkovsky effect also becomes negligible in the limit of infinitely fast rotation because surface temperature variations are smeared along lines of constant latitude and zero rotation.
- Size dependence: The Yarkovsky effect vanishes for both very small and very large objects. For large objects, $(da/dt) \approx \Theta/R'$, where the $\approx 1/R$ dependence arises from the body's cross-section versus its mass. For small objects, $(da/dt) \approx R'^2/\Theta$. The maximum drift in a occurs when $R' \approx 1$ (i.e., when the body's size is comparable to the penetration depth of the corresponding thermal wave). These trends can be seen in **Figure 2*a***, where we plotted the average Yarkovsky-driven semimajor axis displacement (Δa) of main belt bodies. The objects were started with random obliquities (γ) and a variety of K values.
- Surface-conductivity dependence: Surface conductivity K is the main thermal material parameter modifying the strength of the Yarkovsky effect. It is believed to range from very low values for highly porous or regolith-like surfaces (≈ 0.001 W m^{-1} K^{-1}), to moderate values for bare-rocks such as ordinary chondrites or icy objects (≈ 1 W m^{-1} K^{-1}), up to high values for iron-rich objects like iron meteorites (≈ 40 W m^{-1} K^{-1}). Variations of K modify ℓ_ν and Θ_ν. At low conductivities, we expect that Θ will be small and R' large because the penetration depth of the corresponding thermal wave decays to zero. Thus, $(da/dt) \approx \Theta$ and the Yarkovsky effect disappears. For high conductivities, the thermal parameter diverges and the scaled radius of the body tends to zero because the penetration depth of the corresponding thermal wave diverges. Thus, $(da/dt) \approx R'^2/\Theta$, yielding very fast decay of the Yarkovsky effect as the body

is driven toward thermal equilibrium. Maximum da/dt rates occur when both $R' \approx 1$ and $\Theta \approx 1$.

- Solar-distance dependence: The Yarkovsky effect decreases with increasing distance from the Sun. In case of the diurnal effect, objects are usually in the high-Θ and high-R' regime, so that $(da/dt) \approx \Phi/(n\Theta)$. From the functional dependence of Φ, n, and Θ on a, we find that $(da/dt) \approx a^{-2}$ (e.g., Radzievskii 1952, Peterson 1976). Thus, the diurnal effect decreases quickly as distance from the Sun increases, with very slowly rotating bodies a possible exception. A comparable analysis for the seasonal effect is more involved because F_n cannot be approximated as $\approx 1/\Theta$. An example of this would be 0.1–1 km icy bodies in the Kuiper belt, whose seasonal da/dt drift rates become much shallower as a function of distance from the Sun. This surprising result occurs because the penetration depth of the seasonal thermal wave ℓ_n increases to ~ 0.1 km.

Figure 2*b* shows some examples of how the mean distance traveled by bodies are affected when we account for the effect of collisional spin axis reorientation events, disruptive collisions, and the Yarkovsky effect (see also Farinella & Vokrouhlický 1999). Here we assume the bodies experience spin axis reorientation events via nondisruptive impacts with a characteristic timescale $\tau_{rot} \simeq 15.0\sqrt{R}$ My (Farinella et al. 1998). The mean collisional lifetimes of the bodies were taken from Bottke et al. (2005b). We found that the maximum expected drift distance is ~0.1 AU, and that the seasonal Yarkovsky effect allows high K objects to have maximum mobility for $D \approx 10$–20 m (Farinella et al. 1998, Rubincam 1998). For $K = 0.01$ W m^{-1} K^{-1}, the mean drift distances are roughly constant over the D range tested.

4. DIRECT MEASUREMENT OF THE YARKOVSKY EFFECT

The earliest measurements of the strength of the Yarkovsky effect came from the LAGEOS satellite, which was designed for high-precision laser ranging (e.g., Rubincam 1987, 1988, 1990). The Yarkovsky effect has also been measured on asteroids using radar ranging data from the Arecibo and Goldstone radio telescopes (Chesley et al. 2003). Chesley et al. examined a $D = 0.53$ km NEO called (6489) Golevka, which has experienced several close encounters with Earth over the past 15 years. They found that the nongravitational acceleration experienced on Golevka was consistent with the Yarkovsky theory (e.g., Vokrouhlický et al. 2000, 2001b), with their best-fit values yielding a bulk density of 2.7 ± 0.2 g cm^{-3} and $K \sim 0.01$ W m^{-1} K^{-1}. Thus, Yarkovsky measurements via radar ranging and optical astrometry offer scientists a new way to constrain the physical properties of NEOs, with a dozen or more opportunities available over the next decade (Vokrouhlický et al. 2005a,b).

A different approach was taken by Nesvorný & Bottke (2004), who used the orbital distribution of the Karin cluster, an S-type asteroid family that is 5.8 ± 0.2 My old (Nesvorný et al. 2002a), to determine how the Yarkovsky effect affects multi-kilometer main belt asteroids. Using numerical methods, they determined the da/dt drift speed of ~70 Karin cluster members ($D = 1-6$ km). The magnitude of the measured speeds was again consistent with predictions made by theoretical models and those made of

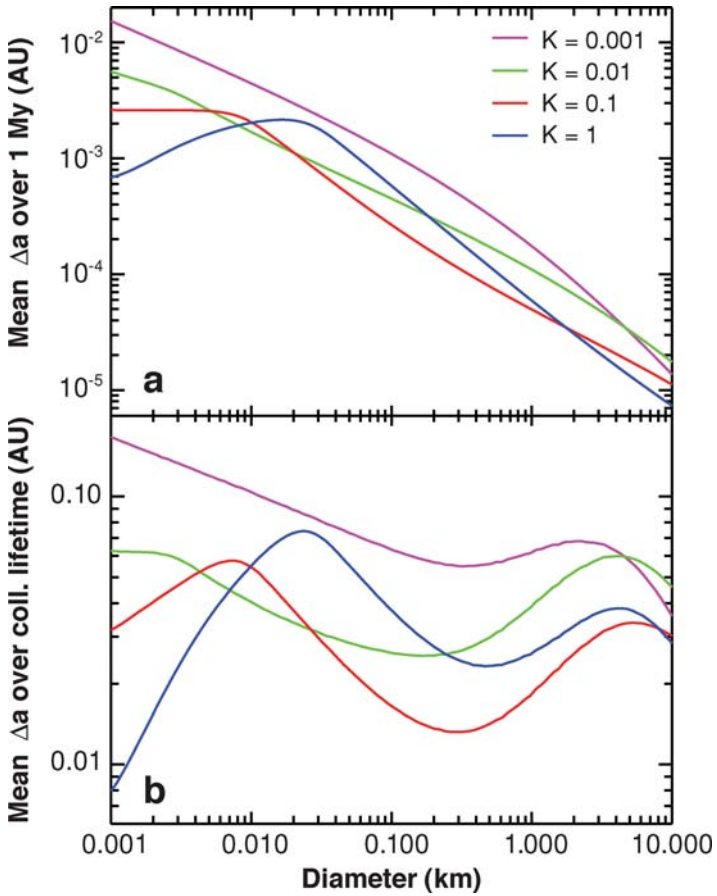

Figure 2

(*a*) Mean drift rate of asteroids in the inner main belt over 1 My produced by the diurnal and seasonal Yarkovsky effects. Surface conductivity K values are 0.001, 0.01, 0.1, and 1 W m^{-1} K^{-1}. Specific heat $C_p = 680$ J kg^{-1} K^{-1}, whereas surface and bulk densities are 1.7 and 2.5 g cm^{-3}, respectively. Rotation period $P = 5$ (D/2), where P is the rotation period in seconds and D the diameter in meters. The low-K cases are dominated by the diurnal effect, whereas for high-K cases the seasonal effect is more important. Mobility decreases for small bodies with high K because the thermal wave penetrates throughout the body. (*b*) Mean change in semimajor axis over the estimated collisional lifetimes of the bodies (Bottke et al. 2005b). Collisions are also assumed to reorient the spin vector of the bodies (Farinella et al. 1998; see text). Note that $D > 1$ km asteroids move farther than in previous work (Farinella & Vokrouhlický 1999) because the assumed collisional lifetimes are longer.

Golevka (Chesley et al. 2003). By comparing the determined drift speeds to the ones calculated from theoretical models, Nesvorný & Bottke (2004) found these bodies have K values consistent with regolith-covered surfaces ($\lesssim 0.1$ W m^{-1} K^{-1}). From the direction the bodies drifted, they also determined that most $D \gtrsim 3.5$ km family members are retrograde rotators, whereas the $D \lesssim 3.5$ km bodies have obliquities

more equally distributed between 0°–180°. These data may be used to study asteroid spin states produced by catastrophic disruption events.

5. APPLICATIONS OF THE YARKOVSKY EFFECT

5.1. Meteorite Delivery

One of the first proposed applications of the Yarkovsky effect was to explain how small bodies are transported from the main belt to Earth (Öpik 1951, Radzievskii 1952, Peterson 1976). It was hypothesized that the Yarkovsky effect might deliver meteoroids from the main belt to Earth via a slow decay of their semimajor axes. The timescales involved with this scenario, however, were far too long to be considered practical. Part of the solution to this delivery timescale problem was found in the pioneering works of J.G. Williams (see Wetherill 1979) and Wisdom (1983), who showed that powerful mean-motion and secular resonances in the inner main belt could potentially move main belt bodies onto Earth-crossing orbits in ~1 My. According to the classical model, stony meteorites then only had to be directly injected into resonances by asteroid collisions.

This scenario, however, delivers a large fraction of meteoroids to Earth with CRE ages of a few million years (Farinella et al. 1994, Gladman et al. 1997); values that are inconsistent with the CRE ages of most stony and iron meteorites (e.g., Morbidelli & Gladman 1998). To avoid this problem, Farinella et al. (1998) eliminated direct injection and instead assumed the Yarkovsky effect slowly delivered material to powerful resonances inside the main belt. As these bodies drifted toward a main belt escape hatch, they would be bombarded by cosmic rays, which would push their CRE ages into the appropriate range. In addition, because iron meteorites have very different thermal conductivities than stones, their da/dt rates are slow enough to explain their long CRE ages (0.1–1 Gy). Thus, the Yarkovsky effect provides a natural explanation for the paucity of short CRE ages among stony meteorites and the differences in the observed CRE ages of stony and iron meteorites.

The dynamical evolution of main belt meteoroids can be surprisingly complex. As described in the previous section, the drift rate for meter-sized stones in the main belt is $\pm$(0.01–0.001) AU My^{-1} (**Figure 2**), depending on their spin axis orientation, spin rate, and thermal properties. Numerical integration work (e.g., Alfonso et al. 1995, Bottke et al. 2000) has shown that in cases where thermal conductivity K is low (e.g., ~0.001 W m^{-1} K^{-1}, or where the meter-size body has a dusty/highly porous surface), meteoroid da/dt drift rates are fast enough to allow meteoroids to "jump-over" most weak resonances, effectively accelerating their drift rate. In these cases, meteoroids will spiral inward or outward until they become trapped in a powerful resonance too chaotic to jump (e.g., the 3:1 or ν_6 resonance). En route, some may become temporarily trapped in weak mean-motion or secular resonances, allowing their e and i values to undergo secular changes while a remains fixed. Additional complications come from nondisruptive collisions because they can modify the meteoroid's spin axis orientation and spin rate. Thus, objects drifting via the Yarkovsky effect may well reverse course and speed several times before reaching a powerful resonance.

If K values are high (e.g., >0.1 W m^{-1} K^{-1}, or where the surface is bare rock), meter-sized bodies drift much more slowly, such that many disrupt before reaching a resonance. This means that the bodies reaching resonances are likely the by-products of a "collisional cascade" produced by several generations of disruption events. As an example, consider the creation of an asteroid family with members that are compositionally similar to one another (Cellino et al. 2002). As the family slowly spreads in semimajor axis via the Yarkovsky effect (see Section 5.2), disruption events constantly create new meter-sized bodies while eliminating existing ones. Eventually, this slow but steady evolution allows the outliers of a family to reach a resonance before being disrupted. Thus, in this scenario, large asteroid families capable of providing a steady reservoir of meteoroid-sized material can dominate the flux reaching a given resonance (see Bottke et al. 2005c).

Although the dynamical evolution of individual meteoroids via the Yarkovsky effect requires careful work, the evolution of large "swarms" of fragments, released by catastrophic break-up events or impacts on large asteroids in the main belt, can be modeled statistically. To this end, the most successful effort so far to combine dynamics, collisions, and the Yarkovsky effect into a meteoroid evolution code has been the work of Vokrouhlický & Farinella (2000). In their model, they started with a size distribution of small bodies ejected from a chosen parent asteroid, with each body having its own spin rate and spin axis orientation. Using simplified dynamics, they tracked these bodies across the inner main belt to the 3:1 or ν_6 resonance, assuming that their da/dt drift rates were not influenced by smaller resonances. Collisions were also included, with random impact events producing cascades of new fragments from the disruption of the existing bodies. When the objects reached the 3:1 or ν_6 resonance, Yarkovsky evolution was shut off and the bodies were delivered to Earth via statistical results taken from the numerical simulations of Morbidelli & Gladman (1998).

The combination of the two studied phenomena—Yarkovsky drift and collisional dynamics—was found to efficiently supply the 3:1 and ν_6 resonances with small asteroid fragments from nearly all locations in the inner and central main belt. Direct injections, considered in "pre-Yarkovsky" studies (e.g., Farinella et al. 1993), only appear to be important when a potential source body borders a resonance. Moreover, the flux of objects to the resonances is, contrary to the direct-injection scenario, spread over hundreds of millions of years, as the collisional cascade creates fast-drifting fragments from larger, slower-drifting progenitors. Another important result from this model is that the distribution of accumulated CRE ages in the population of fragments reaching Earth is in reasonable agreement with observations (e.g., Eugster 2003), with the CRE age histograms dependent on the age of the last event capable of dominating the local Earth swarm. **Figure 3** shows a comparison of the simulated and observed CRE ages for different types of meteorites and different parent asteroids.

5.2. Dynamical Spreading of Asteroid Families

Asteroid families are clusters of fragments produced by catastrophic disruption events that have similar proper a, e, and i values (Milani & Knežević 1994, Knežević et al. 2002) and spectral signatures consistent with an origin from a common parent body

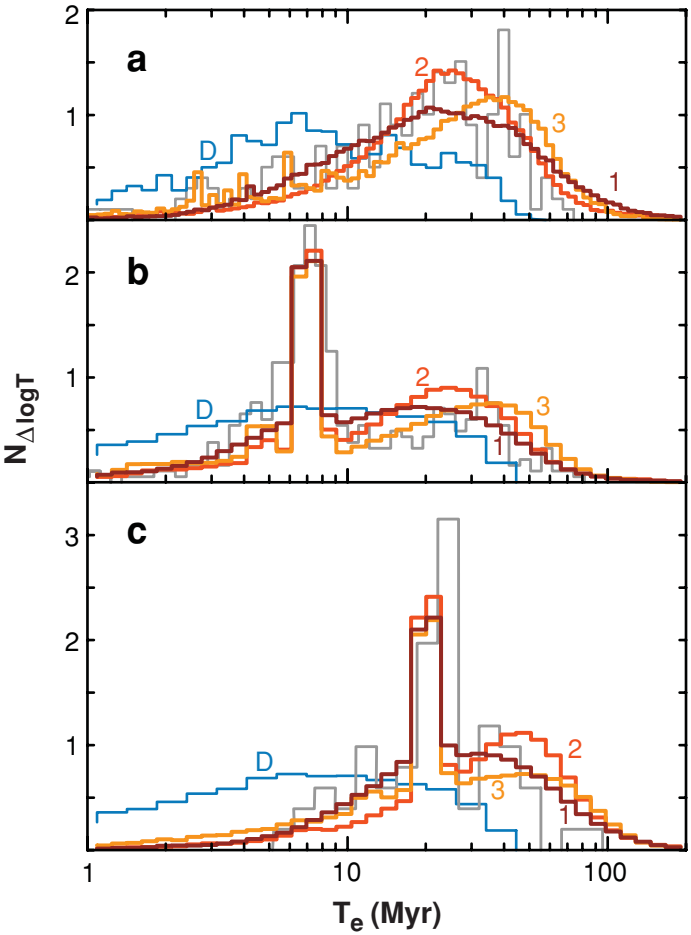

Figure 3

Comparison of the modeled and observed CRE age distributions for three different meteorite types (data—*gray histograms*). We show results of the direct-injection scenario with no Yarkovsky mobility (D histogram, *blue*) and the model including Yarkovsky mobility of the meteoroids and their precursors (*bold full-line histograms*, *orange and red*). Histograms 1, 2, and 3 refer to thermal conductivity values of 0.0015, 0.1, and 1 W m^{-1} K^{-1}, respectively. Part (*a*) assumes ejecta from asteroid Flora whose computed CRE ages are compared with the observed distribution for 240 L-chondrites. Part (*b*) assumes ejecta from asteroid (6) Hebe and the comparison with 444 CRE ages of H-chondrites. Part (*c*) assumes ejecta from asteroid (4) Vesta, compared to the CRE age data for 64 HED (howardite-eucrite-diogenite) meteorites. In all cases, the intermediate *K* value appears to provide the best match to the data. Note that the direct injection scenario would always predict many more short CRE ages than are observed, and a shortage of ages between 20 and 50 My, which is not observed.

(e.g., Cellino et al. 2002). They are important because they are natural laboratories for understanding the physics of hypervelocity impacts. By properly interpreting how families formed and how they evolved, we obtain powerful constraints for numerical hydrocode models (e.g., Benz & Asphaug 1999) and collisional evolution codes (e.g., Bottke et al. 2005a,b), as well as critical clues that allow us to glean insights into the physical properties of asteroids and planetesimals.

As described in the introduction, however, the classical model makes several predictions about asteroid families that are inconsistent with observational and theoretical constraints: (*a*) they predict that the initial ejection velocities of many prominent families were several 100 m s^{-1} (Zappalà et al. 1996); (*b*) they cannot explain the asymmetric (a, e, i) distributions of some families (e.g., the distribution of the Koronis family; **Figure 4**); and (*c*) they cannot explain why some multi-kilometer members of presumably billion-year-old asteroid families are "on the brink" of entering a resonance (e.g., Koronis family members; Milani & Farinella 1995, Knežević et al. 1997, Vokrouhlický et al. 2001a), are already inside powerful resonances (e.g., Eos family members; Zappalà et al. 2000), or are part of the relatively short-lived NEO population (V-type asteroids, which presumably are part of the Vesta family; Migliorini et al. 1997).

One way to resolve these issues is to assume that family members, since their formation, have been spread out in semimajor axis by the Yarkovsky effect. As shown in **Figure 2**, an ensemble of $D = 5$ km asteroids will move inward and outward at mean drift rates of $|da/dt| \sim 2 \times 10^{-5}$ AU My^{-1}, whereas larger asteroids drift more slowly (e.g., $D \sim 20$ km asteroids drift at $|da/dt| \sim 6 \times 10^{-6}$ AU My^{-1}). Because collisional models suggest that many asteroid families are hundreds of millions to billions of years old (Bottke et al. 2005a,b), the potential drift distances of these objects are large enough to explain the observed dispersions of many asteroid families. Moreover, because Yarkovsky drift is size-dependent, the family members would eventually take on the appearance that they were launched using a size-dependent velocity distribution.

Thus, according to this scenario, the observed asteroid families were created through a multi-step process. (*a*) A large asteroid undergoes a catastrophic disruption and ejects fragments at velocities consistent with those found in laboratory experiments and hydrocode simulations. (*b*) $D \lesssim 30$ km fragments, whose initial velocity dispersion is smaller than those currently observed among asteroid families, start drifting in semimajor axis under the Yarkovsky effect. (*c*) $D \lesssim 30$ km fragments jump over or become trapped in chaotic mean motion and secular resonances that change their eccentricity and/or inclination. (*d*) Family members that drift far enough may fall into mean motion or secular resonances capable of pushing them onto planet-crossing orbits. From here, they become members of the Mars-crossing and/or NEO populations.

To check this idea, Bottke et al. (2001) tracked the evolution of test asteroids started close to the center of the Koronis family. **Figure 4** shows Yarkovsky forces driving multi-kilometer asteroids through numerous secular resonances where resonant jumping/trapping events produce noticeable changes in proper e, particularly on the right side of the plot. The most significant jumps are caused by the secular

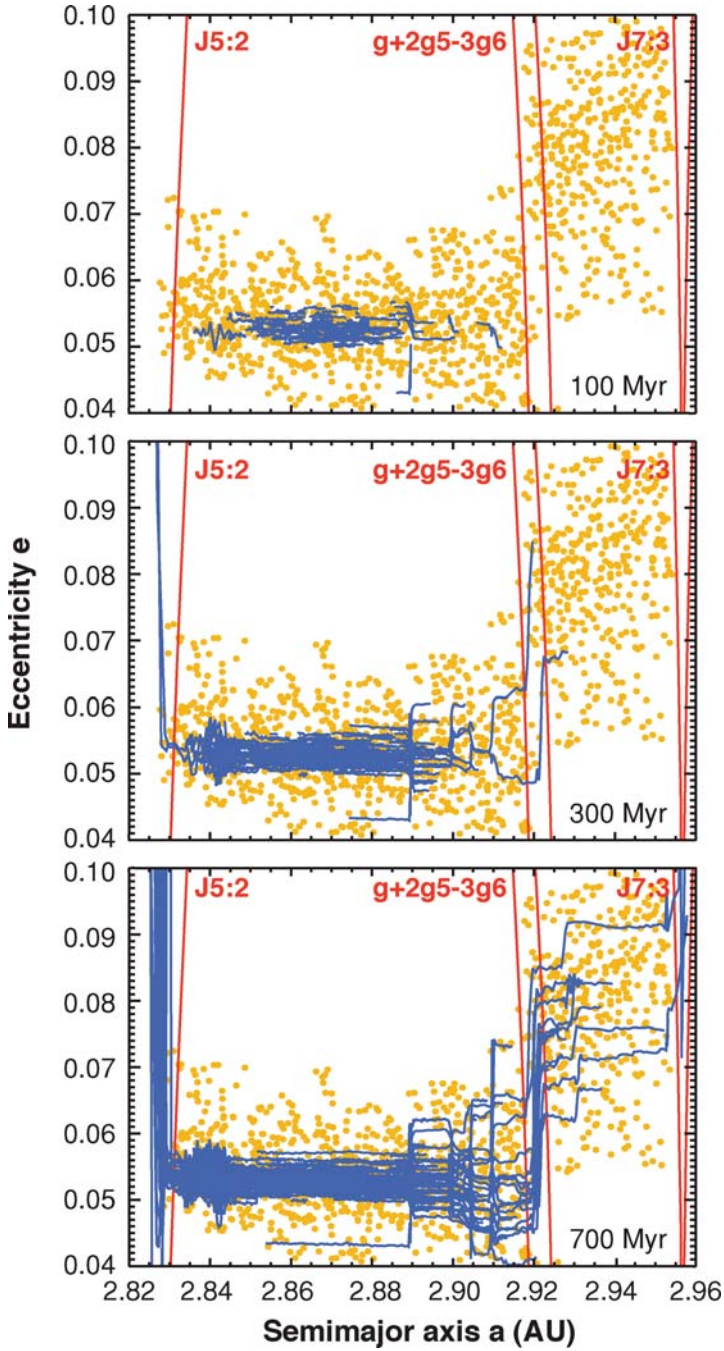

resonance $g + 2g_5 - 3g_6$ at 2.92 AU, which increases e but does not significantly change i. Eventually, objects drifting far enough become trapped in the powerful 5:2 or 7:3 mean motion resonances, where they are pushed onto planet-crossing orbits and are lost from the main belt.

Overall, these integration results reproduce the (a, e, i) distribution of the Koronis family while also explaining the paucity of family members on the left/right sides of the 5:2 and 7:3 resonances and the short-lived nature of some Koronis family members. The success of this model, together with the previous section's results, makes a strong case that the Yarkovsky effect, working in concert with resonances, is the primary mechanism by which $D \lesssim 30$ km asteroids escape the main belt and reach the inner Solar System.

Since Bottke et al. (2001), several groups have investigated the dynamical evolution of families and interesting subpopulations using numerical methods. We highlight the results from some of these studies:

- Tsiganis et al. (2003) analyzed the population of asteroids residing inside the 7:3 mean motion resonance that brackets Koronis family (e.g., **Figure 4**). They noted that this population, made up of 23 known objects, can be divided into two groups, a low-i group coming from the Koronis family and a high-i group coming from the Eos family (2.96–3.12 AU). Their work showed that the expected delivery rate of multi-kilometer asteroids to the 7:3 resonance from these families via the Yarkovsky effect was sufficient to explain both resident populations. Using a similar model, Brož et al. (2005) succeeded in matching the parameters of asteroids on unstable orbits within the 2:1 mean motion resonance with Jupiter. It is believed these bodies are resupplied over time by asteroids from the Themis and Hygiea families and from the population of nonfamily asteroids adjacent to the 2:1 resonance.
- The Eos family, which has an unusual shape in (a, e, i) space and is intersected by the 9:4 mean motion resonance with Jupiter, provides an opportunity for one to investigate several aspects of the Yarkovsky evolution model. Like Koronis, the portion of the Eos family closest to the Sun is bracketed by a powerful resonance (7:3 resonance at ~2.95 AU), whereas the portion of the family furthest from the Sun lies beyond a relatively weak resonance (9:4 resonance at

Figure 4

Evolution of 210 simulated Koronis family members via the Yarkovsky effect (Bottke et al. 2001). The test family members (*blue lines*) were started within ~60 m s^{-1} of (158) Koronis (proper elements $a = 2.87$ AU, $e = 0.045$, $\sin i = 0.038$) and were integrated for ~700 My, short compared with the estimated age of the family (~2.5 Gy), but enough to determine evolution trends. The orbital tracks were averaged over a running 10 My window to compare them with the proper (a, e) of the Koronis family members (*yellow dots*). Snapshots of the integration tracks, shown at 100 My, 300 My, and 700 My, indicate these bodies interact with several resonances between 2.89–2.93 AU, with the secular $g + 2g_5 - 3g_6$ resonance at 2.92 AU being most prominent. These jumps allow the simulated family members to reach the (a, e) positions of many real family members. Fast-drifting bodies are seen to escape the main belt via the 5:2 and 7:3 mean motion resonances with Jupiter.

~3.03 AU) and is underpopulated. Vokrouhlický et al. (2005c) has shown than the underpopulated region corresponds to the likelihood that an outward drifting asteroid will jump across (as opposed to becoming trapped) in the 9:4 resonance. The family also has an unusual feature produced by family members that become trapped at low-i by the high-order secular resonance $z_1 = s + g - s_6 - g_6$. The most curious element of the Eos family, however, is that the center of the family is depopulated in small family members relative to that found on the extremes. This is likely a consequence of combined Yarkovsky/YORP evolution, where the Yarkovsky drift rates are intimately tied to the obliquity evolution produced via the YORP effect (see Sections 6–7).

- The dispersion of the Flora family was investigated by Nesvorný et al. (2002b), whereas the Gefion and Adeona families were investigated by Carruba et al. (2003). In addition to Yarkovsky evolution, both groups examined whether close encounters with large asteroids like (1) Ceres, (2) Pallas, and (4) Vesta could affect the orbital evolution of $D > 20$ km family members, objects that are less susceptible to Yarkovsky evolution than their smaller brethren. Overall, they found that asteroidal close encounters have a small effect on the spreads of asteroid families as a whole, but that a small fraction ($\lesssim$10%) of each family did experience meaningful changes in semimajor axis.

5.3. Escape of Kilometer-Sized Asteroids from the Main Belt

Dynamical modeling results indicate that the ultimate source of most Mars-crossing asteroids and NEOs is the inner/central main belt (e.g., Bottke et al. 2000a, 2002a). The primary sources of these bodies are the 3:1 mean-motion resonance with Jupiter at 2.5 AU, the ν_6 secular resonance that brackets the main belt in inclination from 2.1 – 2.5 AU, and numerous narrow mean motion resonances produced by Mars or the combined effects of Jupiter and Saturn, which span the entire length of the main belt (Wisdom 1983, Morbidelli & Gladman 1998, Migliorini et al. 1998, Morbidelli & Nesvorný 1999). The question, however, is how main belt material reaches these resonances.

In the CM, asteroids were thrown directly into resonances by main belt collisions (e.g., Farinella et al. 1993). Catastrophic disruption events in the main belt, however, occur relatively infrequently; only ~20 asteroids with $D > 100$ km have disrupted over the past 3–4 Gy (Bottke et al. 2005a,b). Moreover, the combined width of resonances in the inner and central main belt is small enough that collisions alone are unlikely to keep them filled with debris (Farinella & Vokrouhlický 1999). Finally, the mean dynamical lifetimes of material injected into the resonances described above are only a few million years (Gladman et al. 1997, Bottke et al. 2002b), such that a shortage of resonant material could eventually lead to a discernible depletion of inner solar system asteroids (Migliorini et al. 1998, Michel et al. 2000). These problems are exacerbated by the fact that most potential parent bodies are located far from resonant escape hatches (Nesvorný et al. 2002a), and that the disruption of large bodies in the inner main belt should produce numerous asteroid families that are not observed (e.g., Nesvorný et al. 2003).

For these reasons, Farinella & Vokrouhlický (1999) postulated that most main belt resonances are restocked with $D \lesssim 30$ km asteroids via the Yarkovsky effect. This potential solution could explain the spectral diversity of the inner Solar System asteroid population (e.g., Binzel et al. 2004) as well as the slope of its size-frequency distribution, which is shallower [$N(> D) \propto D^{-1.75}$; Bottke et al. 2000a] than one might expect if fresh ejecta were being launched directly into resonances [$N(> D) \propto D^{-3\,\mathrm{to}\,-4}$; Tanga et al. 1999].

To test this idea, Bottke et al. (2002b) numerically integrated hundreds of test asteroids with $D = 0.2$, 0.4, 2, 4, and 10 km in the inner (2.1–2.48 AU) and central (2.52–2.8 AU) main belt with and without the Yarkovsky effect. The orbits of the test asteroids were chosen to be a representative sample of the observed population residing near (but not on) Mars-crossing orbits (perihelion $q \gtrsim 1.8$ AU; Migliorini et al. 1998, Morbidelli & Nesvorný 1999). All the test asteroids were given thick regoliths and low thermal conductivity K values, although it is not yet clear whether this approximation is reasonable for small asteroids. Bottke et al. found that Yarkovsky-driven objects with $D > 2$ km reached Mars-crossing orbits at the same rate as the non-Yarkovsky case, with most objects having their e values increased by interactions with multiple tiny resonances. For $D < 2$ km objects, however, their drift rates are apparently fast enough that most of these test asteroids jumped across numerous weak resonances en route to the 3:1 and ν_6 resonances or the Mars-crossing region.

Investigating this problem in a different way, Morbidelli & Vokrouhlický (2003) used a Monte-Carlo code to track how the population of NEOs delivered from the inner main belt changed over time. In their code, they created a simplified model of the orbital and size distribution of the inner main belt population ($a < 2.5$ AU), with the asteroid population estimated from observational data (e.g., Minor Planet Center). Next, they followed the semimajor axis evolution of their test objects, with random deviates used to assign their initial spin vectors as well as the timing of spin vector reorientation and catastrophic collision events; note that spin vectors control the direction and magnitude of Yarkovsky da/dt rates. When the test asteroids reached the 3:1 or ν_6 resonance, they were removed and replaced by same-size test asteroids that were started from the same location the removed asteroids came from. Morbidelli & Vokrouhlický (2003) found that they could reproduce the flux needed to keep the NEO population in steady state (220 multikilometer asteroids per million years; Bottke et al. 2002a). They also found that the Yarkovsky effect steepens the power law slope of the NEO size distribution for $1 < D < 10$ km bodies, naturally explaining the differences seen between the main belt [$N(> D) \propto D^{\alpha}$, with $\alpha = -1.3$] and NEO populations ($\alpha = -1.75$) in this size range. Interestingly, their evolution model had to include the YORP effect to match the NEO size distribution (see Section 6).

Finally, we have the work of La Spina et al. (2004), who investigated the spin axis orientations of the observed NEOs. They found that 15 of the 21 NEOs with known obliquities are retrograde rotators (71%), in excess of what one would expect from a random distribution. This data set provides surprisingly strong support for the idea that NEOs evolve out of the main belt via the Yarkovsky effect. Using a numerical model of the NEO population, Bottke et al. (2000a, 2002a) estimated that $37 \pm 8\%$ of kilometer-sized NEOs come from the ν_6 resonance, with the remainder coming

from a variety of resonances spread across the main belt. Because the ν_6 resonance defines the innermost boundary of the main belt, however, it can only be reached by objects evolving inward toward the Sun. In terms of Yarkovsky *da/dt* drift, these objects must have retrograde spins. All the remaining resonances in the main belt can be reached by objects drifting either inward or outward (i.e., prograde and retrograde spins). Thus, if 100% of the NEOs coming out of the ν_6 resonance have retrograde spins, and the rest are split 50–50 between prograde and retrograde, the fraction of the NEO population having retrograde spins is 69%, a remarkable match with observations [71%, according to La Spina et al. (2004)].

6. THE YORP EFFECT: MODIFYING ASTEROID SPIN RATES AND OBLIQUITIES

The reflection and reemission of sunlight from an asteroid's surface can also produce a net thermal torque on asteroids with irregular shapes. Over time, these torques can affect the spin rate and obliquities of small bodies in the Solar System, driving some of them toward asymptotic values. This "sunlight alters spin" mechanism was coined by Rubincam (2000) as the YORP effect (Radzievskii 1954; Paddack 1969, 1973; Paddack & Rhee 1975; O'Keefe 1976). YORP is important because it not only controls the long-term evolution of asteroid spin vectors but also the magnitude and direction of Yarkovsky *da/dt* rates, which depend on rotation parameters. In fact, when its effects are combined with the related Yarkovsky effect, YORP may help to explain several puzzling issues about the rotational, orbital, and physical parameters of small asteroids (Bottke et al. 2002b, Rubincam 2000, Rubincam et al. 2002, Vokrouhlický & Čapek 2002, Morbidelli & Vokrouhlický 2003). We may also be able to directly detect YORP through a measurable change in phase of the sidereal rotation of small asteroids (Vokrouhlický et al. 2004).

Rubincam (2000) illustrated how YORP works using a rotating spherical asteroid with two wedges attached to the equator (**Figure 5**). For a Lambertian radiator, the reaction force from photons departing from any given element of area will be normal to the surface, such that no torque is produced. Energy reradiated from the wedges, however, does produce a torque because the wedge faces are not coplanar. For the sense of rotation shown in **Figure 5**, the wedge-produced YORP torque spins the object up. If the body happened to spin in the opposite sense, the YORP torques would slow it down. Thus, an object must have some "windmill" asymmetry for YORP to work; energy reradiated from a symmetrical body (e.g., a sphere or an ellipsoid) produces no net YORP torque (Rubincam 2000, Bottke et al. 2002b, Vokrouhlický & Čapek 2002).

YORP torques can also modify asteroid obliquities, which leads to the concept of the YORP cycle. For the geometry shown in **Figure 5**, a fast-spinning asteroid would gradually increase its obliquity as well. When the obliquity becomes large enough, the axial torque changes sign and the object begins to spin down. This can be seen by imagining that the Sun shines down on the object from its north pole, rather than the equator; the wedges must spin it the other way. Hence YORP may spin objects up for a while, but when the obliquity becomes large, they slow down and then perhaps

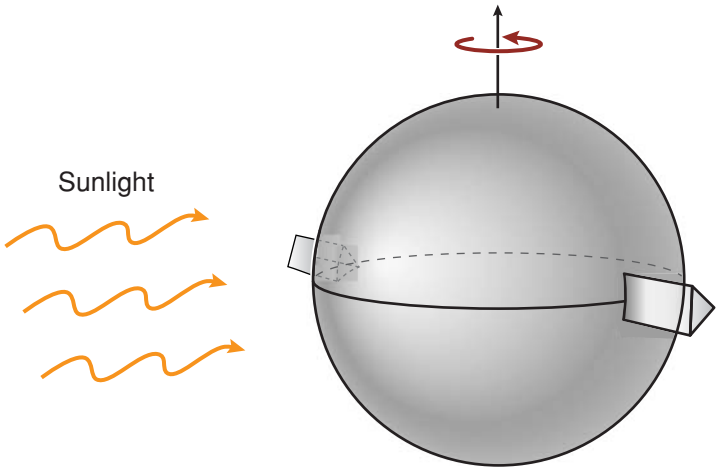

Figure 5

Spin up of an asymmetrical asteroid. The asteroid is modeled as a sphere with two wedges attached to its equator. The asteroid is considered a blackbody, so it absorbs all sunlight falling on it and then reemits the energy in the infrared as thermal radiation. Because the kicks produced by photons leaving the wedges are in different directions, a net torque is produced that causes the asteroid to spin up.

tumble until they reestablish principal axis rotation, with the spin axis presumably pointing in a random direction. Then the cycle begins all over again, such that small solid objects possibly avoid the "rotational bursting" envisioned by V.V. Radzievskii, S.J. Paddack, and J.A. O'Keefe (i.e., spinning an solid object so fast that it disrupts). Collisions large enough to modify an asteroid's spin axis orientation may also short-circuit a YORP cycle, potentially putting the object into an entirely different rotation state. Thus, YORP is most likely to be important in regimes where the YORP cycle is faster than the spin axis reorientation timescale via collisions (Rubincam 2000, Vokrouhlický & Čapek 2002, Čapek & Vokrouhlický 2004).

6.1. Theory of the YORP Effect

YORP, like the Yarkovsky effect, can be thought of as a recoil force $d\mathbf{f}$ applied to a surface element $d\mathbf{S} = \mathbf{n}_\perp \, dS$ produced by the thermal reflection and reemission of absorbed sunlight (Equation 3). By integrating $d\mathbf{f}$ over the entire surface S of asteroid, we obtain the net thermal torque:

$$\mathbf{T} = \int \mathbf{r} \times d\mathbf{f}, \tag{7}$$

where $\mathbf{r}$ is the position vector of the appropriate surface element $d\mathbf{S}$ in Equation 3. In practice, the irregular shapes of asteroids are modeled using a polyhedral surface composed of N triangular facets (typically $N \geq 10^3$; e.g., Simonelli et al. 1993, Dobrovoskis 1996, Vokrouhlický & Čapek 2002). The YORP torque is the sum of the torques produced by the triangular surface elements. The major unknown

quantity in Equation 7 is the surface temperature T, which depends on several factors: the incident solar radiation on each surface element, which depends on factors like the asteroid's orbit, shape, etc.; the body's reflectivity in the optical band, which is expressed by the albedo coefficient A; and how solar radiation is conducted into the body. To attain the highest accuracy (e.g., Čapek & Vokrouhlický 2004), we need to compute T numerically for every surface element over time by solving the heat diffusion problem with appropriate boundary conditions (Equation 2). As a rough approximation, one can assume zero thermal conductivity where thermal radiation is emitted with no time lag (i.e., this is a fundamental difference between the Yarkovsky and YORP effects). Here $\varepsilon\sigma T^4 \approx (1-A)\Phi\,(\mathbf{n}\cdot\mathbf{n}_0)$, where Φ is the solar radiation flux on the surface element with normal vector $\mathbf{n}$ along direction $\mathbf{n}_0$ (Rubincam 2000, Vokrouhlický & Čapek 2002).

Assuming the asteroid rotates around the shortest axis of the inertia tensor (with the moment of inertia C), we define $\mathbf{L} = C\omega\,\mathbf{e}$ as the body's angular momentum. Here ω is the angular velocity of rotation and $\mathbf{e}$ is the unit vector of the spin axis. The rate of change of $\mathbf{L}$ in the inertial frame is equal to the applied torque $\mathbf{T}$: $d\mathbf{L}/dt = \mathbf{T}$. For C constant, this equation can be split into

$$\frac{d\omega}{dt} = \frac{\mathbf{T}\cdot\mathbf{e}}{C} \equiv \frac{T_s}{C}, \tag{8}$$

$$\frac{d\mathbf{e}}{dt} = \frac{\mathbf{T} - (\mathbf{T}\cdot\mathbf{e})\,\mathbf{e}}{C\omega}. \tag{9}$$

It is useful to parametrize the spin vector $\mathbf{e}$ with the obliquity ϵ, the angle between $\mathbf{e}$ and normal vector $\mathbf{N}$ to the orbital plane, and the precession in longitude ψ. The decomposition of $\mathbf{e}$ into orbital plane unit vectors (x-coordinate along the nodal line) then becomes $(\sin\epsilon\,\sin(\psi+\Omega), \sin\epsilon\,\cos(\psi+\Omega), \cos\epsilon)$, where Ω is the longitude of ascending node. We can then write

$$\frac{d\epsilon}{dt} = \frac{\mathbf{T}\cdot\mathbf{e}_{\perp 1}}{C\omega} \equiv \frac{T_\epsilon}{C\omega}, \tag{10}$$

$$\frac{d\psi}{dt} = \frac{\mathbf{T}\cdot\mathbf{e}_{\perp 2}}{C\omega} \equiv \frac{T_\psi}{C\omega}, \tag{11}$$

with the unit vectors

$$\mathbf{e}_{\perp 1} = \frac{(\mathbf{N}\cdot\mathbf{e})\,\mathbf{e} - \mathbf{N}}{\sin\epsilon}, \qquad \mathbf{e}_{\perp 2} = \frac{\mathbf{e}\times\mathbf{N}}{\sin\epsilon}. \tag{12}$$

Note that in reality $\mathbf{T}$ not only includes the YORP torque but also the gravitational torque due to the primary and/or inertial terms due to the motion of the orbital frame used to define the angles ϵ and ψ (e.g., Vokrouhlický & Čapek 2002). The gravitational and inertial terms, however, usually dominate the precession component T_ψ. Conversely, their long-term contributions to T_s and T_ϵ are negligible, whereas YORP produces nonzero secular effects in the rotation speed and obliquity. For this reason, we concentrate on these thermal torque components when computing how YORP affects an asteroid. Moreover, because YORP torques act over long timescales, we can average T_s and T_ϵ over their rotation and revolution cycles.

7. COMPUTING THE YORP EFFECT FOR INDIVIDUAL ASTEROIDS

Rubincam (2000) showed that YORP is strongly dependent on an asteroid's shape, size, distance from the Sun, and orientation. For example, assuming the Sun remains on the equator, asteroid (951) Gaspra, with radius $R = 6$ km and $a = 2.21$ AU, would take 240 My to go from a rotation period $P = 12$ h to 6 h (and vice versa). We call this value the YORP timescale. If (243) Ida had the the same R and a values as Gaspra, it would have a YORP timescale half as long, whereas a body with Phobos' shape would have a YORP timescale of several billion years. Clearly, shapes make a big difference. The YORP timescale is also size-dependent (i.e., it goes as $\approx R^2$), such that smaller sizes spin up much more quickly. If Gaspra was only $R = 0.5$ km, its YORP timescale would be a few million years. Thus, YORP may be very influential for kilometer-sized and smaller asteroids. YORP is also more effective as you move closer to the Sun. Moving our $R = 0.5$ km Gaspra to 1 AU allows it to go from $P = 12$ h to rotational disruption speeds of $\sim$2 h (and visa-versa) in $\sim$1 My. We caution, however, that YORP-induced obliquity torques may double or possibly triple the above timescales (see below). Moreover, these rates ignore complications such as collisions, planetary close encounters, changes in thermal properties with size, etc.

To demonstrate how YORP modified the spin vectors of individual asteroids, we show results from Čapek & Vokrouhlický (2004), who examined several bodies with well-determined shapes. Here we focus on (6489) Golevka, whose detailed shape model was obtained using radar ranging echoes in 1995 (Hudson et al. 2000, see also Chesley et al. 2003). For simplicity, they assumed their model Golevka resides on a circular orbit with $a = 2.5$ AU, bulk density of 2.5 g cm^{-3}, surface density of 1.7 g cm^{-3}, specific heat capacity $C_p = 680$ J kg^{-1} K^{-1}, and albedo $A = 0$.

An important feature of YORP-driven evolution is that the spin axis gradually tilts toward a specific (asymptotic) obliquity value (Rubincam 2000, Bottke et al. 2002b, Vokrouhlický & Čapek 2002). En route to that obliquity state, the asteroid increases or decreases its rotation rate. This can be seen in **Figure 6**, which shows mean rate of change of the angular velocity and obliquity produced by YORP for a number of surface conductivity K values in the range 10^{-9} to 10 W m^{-1} K^{-1}. For reference, a $K \simeq 0.01$ W m^{-1} K^{-1} is consistent with a surface characterized as a mixture of dusty areas and exposed porous rocks (Chesley et al. 2003). We see that the angular velocity is nearly independent of the angular YORP's torque (T_s/C) on K, whereas there is a strong dependence of the obliquity YORP's torque (T_ϵ/C) on K. If Golevka is given a low K value, its obliquity could potentially evolve to three asymptotic states: 0°, 90° and 180° (Vokrouhlický & Čapek 2002). For $K \geq 5 \times 10^{-5}$ W m^{-1} K^{-1}, however, it can only reach a single asymptotic state at 90°. If we assume $K = 0.01$ W m^{-1} K^{-1} in accordance with Chesley et al. (2003), we find the mean value of the fractional change of the rotation period P, $(dP/dt)/P \simeq -2.2 \times 10^{-7}$ year^{-1} (e.g., Vokrouhlický et al. 2005c). Hence, if enough precise observations are taken over the next decade or so, we may be able to detect YORP on Golevka. A discussion of this and other YORP effect detection possibilities can be found in Čapek & Vokrouhlický (2004) and Vokrouhlický et al. (2004).

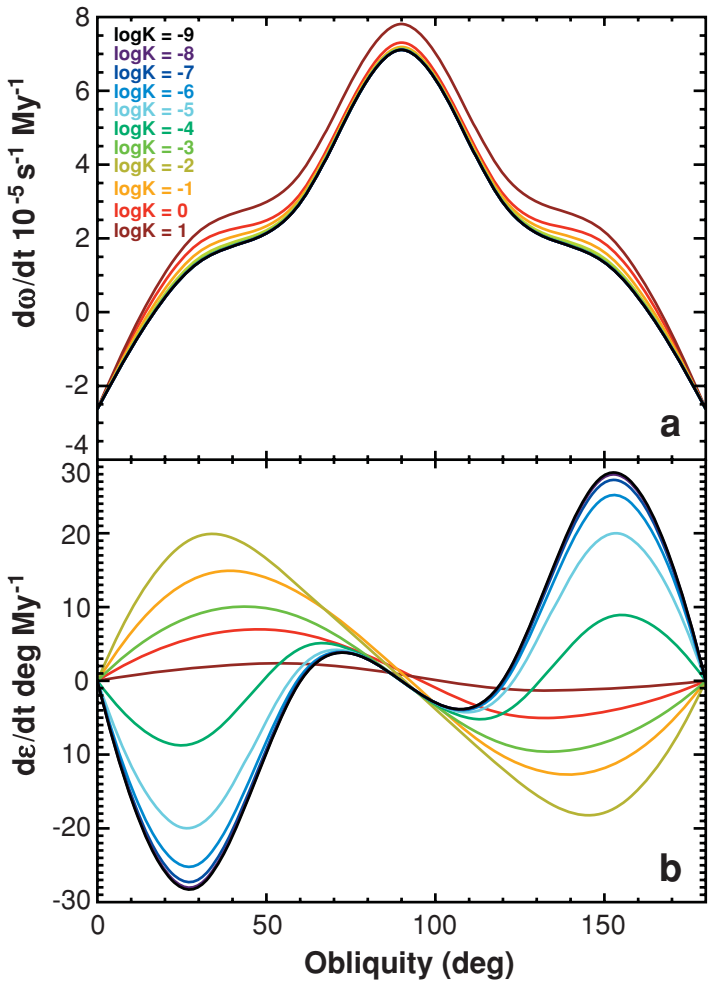

Figure 6

YORP-induced mean rate of change of the rotation rate ω and obliquity ϵ as a function of the obliquity for asteroid (6489) Golevka (assumed to be on a circular orbit at 2.5 AU). Eleven values of the surface thermal conductivity $\log K = -9, -8, \ldots, -1, 0, 1$ are shown. The lowest value—black—is identical to the zero-conductivity case analyzed by Vokrouhlický & Čapek (2002). The rotation effect shows a small dependence on K, whereas the obliquity effect has a significant dependence on K (and rotation period of 6 h).

7.1. Asteroids in Spin-Orbit Resonances

An interesting and potentially important application of the YORP effect has been to understand the spin vectors of Koronis family members. In general, laboratory and numerical experiments of asteroid collisions suggest that Koronis family members, which are likely billions of years old (e.g., Bottke et al. 2001), should have spin rates that approximately follow a Maxwellian distribution and nearly random spin axis

orientations. The observed rotation states of $D = 20$–40 km asteroids within this family, however, are surprisingly discordant with these expectations. Slivan (2002; see also Slivan et al. 2003) found that the prograde rotators had tightly clustered values in spin period ($7.5 < P < 9.5$ h), obliquity ($42^\circ < \epsilon < 50^\circ$), and possibly ecliptic longitude, with the latter two implying the spin axes of this group are truly parallel in space. We refer to prograde objects with spin vectors near these clustered values as being in "Slivan states." Retrograde rotators, on the other hand, had $P <$ 5 h or $P > 13$ h, $\epsilon \geq 154^\circ$, and ecliptic longitudes that appear to span a large range of values. Given the singular nature of the spin vectors in both the prograde and retrograde groups, we consider it unlikely that collisions alone could have produced this distribution; some other explanation is needed.

To explain these spin vectors, Vokrouhlický et al. (2003) constructed a numerical model capable of tracking the spin vector evolution of model asteroids over several billion years via two effects: (*a*) YORP and (*b*) the effects of solar gravitational torques on an asteroid whose orbit changes over time owing to planetary gravitational perturbations. This model was then used to explore the long-term evolution of test Koronis family asteroids with $20 < D < 40$ km and prograde/retrograde spins using both real and artificial asteroid configurations (e.g., the spacecraft-derived shape of (243) Ida, numerous random asteroid shapes derived using numerical techniques; Muinonen 1998).

For prograde rotators, Vokrouhlický et al. (2003) found that Koronis family members predominately spin down, which, in the cases analyzed by Vokrouhlický et al., gave them the opportunity to be captured by spin-orbit resonances. Some representative model cases are shown in **Figure 7**. For retrograde rotators, YORP drove the obliquity values of our test asteroids toward the asymptotic value of $\epsilon = 180^\circ$. By varying the initial P, ϵ values of the test asteroids, and by giving them different shapes, Vokrouhlický et al. found a variety of possible evolutionary paths. Some test asteroids always spin down, whereas others always spin up. There were even cases where objects start by spinning down but then later spin up (or vice versa).

These results led Vokrouhlický et al. (2003) to conclude that the YORP effect, when combined with planetary perturbations, provides the most plausible means to explain the spin rate and obliquity values of the Koronis family asteroids. Moreover, the fact that the observed prograde rotators were trapped in a spin-orbit resonance implies that collisions played a minimal role in the evolution of their ϵ and P values over the past 2–3 Gy. We can generalize this result to the rest of the main belt; over the past several billion years, the YORP effect has probably been more efficient than collisions at changing the spin rates and obliquities of main belt asteroids with $D <$ 40 km. If true, YORP can provide a natural explanation for the plethora of $D < 40$ km asteroids with extremely fast or slow rotation rates (e.g., Pravec et al. 2002).

The YORP effect may also have far-reaching implications for the physical history of many small asteroids. If kilometer-sized asteroids are predominantly gravitational aggregates (or, as many call them, rubble-pile asteroids; Richardson et al. 2002), or they are as weak as suggested by strength models (Holsapple 2005), YORP may spin some of them up so fast that they change shape, shed mass, or even undergo fission. It may thus provide an important means for producing asteroid satellites among smaller

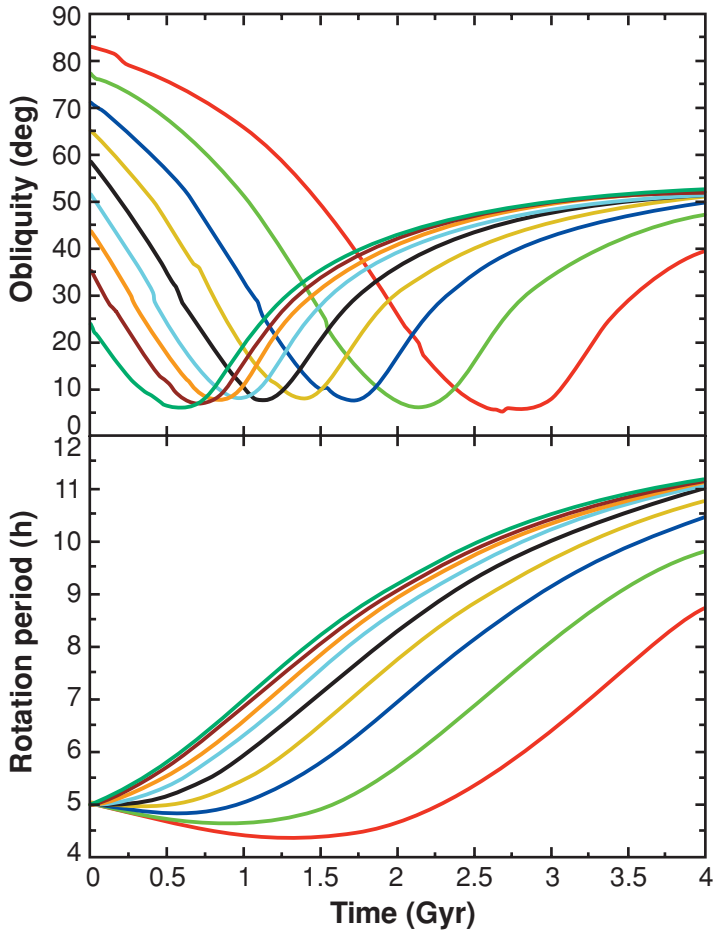

Figure 7

Nine possible evolutionary paths for prograde rotator (311) Claudia ($D = 24$ km; $P = 7.53$ h; $\epsilon = 50°$), many that evolve into resonant states (Vokrouhlický et al. 2003). Claudia's initial spin period was set to $P = 5$ h and its initial obliquity ϵ to uniform values in $\cos\epsilon$ between $0° - 90°$. The YORP torque affecting obliquity, defined as T_ϵ, slowly drives ϵ toward the $0°$ asymptotic value and, in the process, increases $\dot{\psi}$, defined as the asteroid's precession rate with respect to the ecliptic. This occurs because $\dot{\psi} \propto \cos\epsilon/\omega$, where ω is the asteroid's rotation rate. When the initial ϵ is small, or if it becomes so in the course of the evolution, the YORP torque affecting P, defined as T_s, decelerates the rotation rate and therefore also increases the precession rate of the spin axis. Eventually, this motion allows it to becomes captured by the s_6 spin-orbit secular resonance between the precession rate of the asteroid's spin axis and Saturn's longitude of node. We see this occurring near the minimum ϵ values for each curve shown to the left. Once trapped in the resonance, P steadily increases, enough to cause migration of its equilibrium (Cassini) state and force ϵ to move toward the asymptotic value of $\simeq 55°$, where T_s becomes zero for nearly all asteroid shapes.

main belt and near-Earth asteroids. On the other hand, gravitational aggregates may "morph" into new symmetrical shapes that increase the YORP timescale; these shape changes may eventually strand some objects close to the rotational break-up limit.

To investigate whether asteroids in other main belt regions may also be trapped in Slivan states, Vokrouhlický et al. (2003) tracked the spin vector evolution of test prograde rotators having the same orbital parameters as (8) Flora, (15) Eunomia, (20) Massalia, (24) Themis, (37) Fides, and (221) Eos. These asteroids were chosen because they span the main belt in both semimajor axis and inclination. Preliminary results indicate that low inclination asteroids in the outer main belt [e.g., (24) Themis] follow evolutionary paths similar to those described in **Figure 7**; we predict that many more Slivan state asteroids may be found there. For the remaining test asteroids, Vokrouhlický et al. (2003) found more complex spin-vector evolutionary paths brought on, in part, by the presence of overlapping spin-orbit resonances.

7.2. The Ages of Asteroid Families Derived from the Yarkovsky/YORP Effect

Despite our apparent success in using Yarkovsky evolution to interpret asteroid family data, there are still several issues related to families that need to be better understood. For example, the dynamical spreading experienced by family members via Yarkovsky/YORP slowly masks the initial velocity distribution of small and/or old families (Dell'Oro et al. 2004). For this reason, we only have solid ages for very young families. An example is the Karin family, an exceptionally compact cluster of asteroids located inside the Koronis family (Nesvorný et al. 2002a). By numerically integrating the fragments backward in time, Nesvorný et al. showed that Karin family members were produced by the disruption of a $D \sim 30$ km asteroid $\sim 5.8 \pm 0.2$ My ago (see also Nesvorný & Bottke 2004). A similar young age was found for the Veritas family ($\sim$3.17 AU), which was produced by the disruption of a $D > 150$ km asteroid $\sim 8.3 \pm 0.5$ My ago (Nesvorný et al. 2003). Numerical modeling work indicates Veritas was, by far, the largest asteroid disruption event to have occurred over the past 70 My (Nesvorný et al. 2003; Bottke et al. 2005a,b). In fact, it was so large that collisions between family members still produce as much as 10% of all Solar System near-ecliptic dust observed by IRAS (Nesvorný et al. 2005).

To determine the ages of older asteroid families more heavily influenced by Yarkovsky/YORP, Vokrouhlický et al. (2005d) constructed a Monte-Carlo code that can track the evolution of asteroids via Yarkovsky/YORP simultaneously. This code, while not without simplifications, may allow one to distinguish between the competing contributions produced by a family's initial velocity distribution and its dynamical spreading over time. An important implication of this work is that it may be possible to use Yarkovsky/YORP spreading like a clock to determine the formation ages of various families.

As an example, we show results from their analysis of the Erigone family, which was likely produced by the disruption of a $D \sim 110$ km C-type asteroid in the inner main belt ($a \sim 2.37$ AU) (Bottke et al. 2005a,b). A plot of family members in (a, H) space shows it is divided into two fragment clouds separated by a surprising depletion at

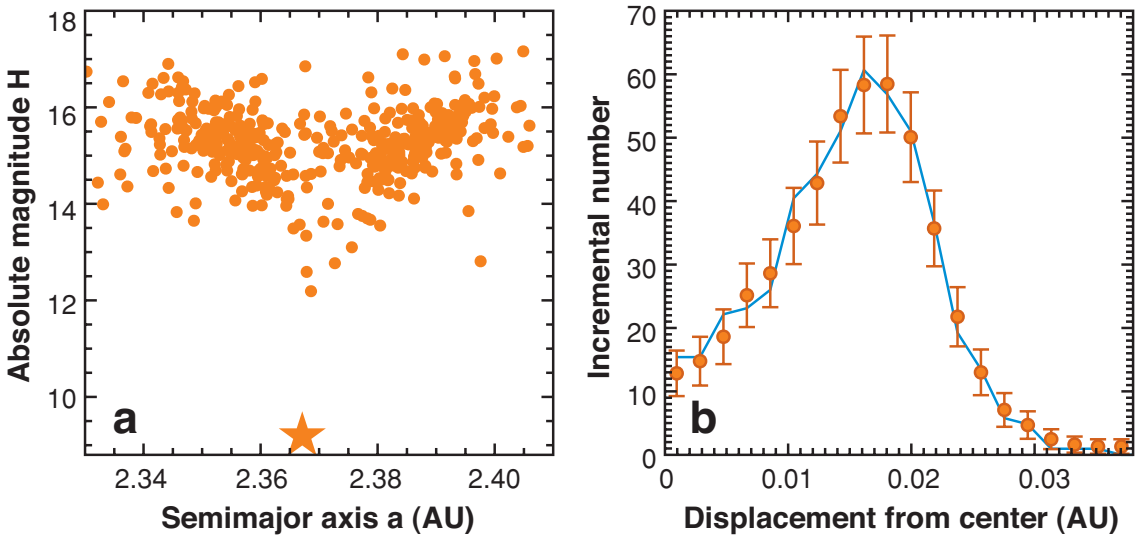

Figure 8

(*a*) The Erigone family projected onto a plane of proper semimajor axis *a* versus absolute magnitude *H*; (163) Erigone is the filled star. We postulate the family has been separated into two clouds ($a \lesssim 2.37$ AU; $a \gtrsim 2.37$ AU) by Yarkovsky/YORP evolution. (*b*) A comparison between model results (*solid blue line*) and binned Erigone family (*filled orange dots*; see Vokrouhlický et al. 2005d). The error bars are the square root of the number of bodies in each bin. The *y*-axis is the distance between the test/observed family members and the family's center. We assumed our test asteroids had a mean albedo of 0.05.

the center (**Figure 8**). Tests indicate this feature is not a by-product of resonances. By fitting their runs to the (a, H) distribution, Vokrouhlický et al. (2005d) estimate that the age of the Erigone family is $T = 280^{+30}_{-50}$ My, whereas the mean ejection velocity of the 5-km size fragments was $V = 26^{+14}_{-11}$ m s^{-1}. Thus, the initial distribution of the Erigone family covered roughly half the distance in semimajor axis as the observed one. We believe the techniques demonstrated in Vokrouhlický et al. (2005d) will ultimately help us determine the ages of families across the main belt.

8. FUTURE DIRECTIONS

While introducing the Yarkovsky/YORP effects into our asteroidal dynamical models has been highly successful, there are still many issues that require future work. One challenge for future Yarkovsky modeling will be to accurately combine Yarkovsky accelerations with YORP, particularly because there is a complicated interaction between rotation, orbit precession rates, and spin axis precession rates. Moreover, as shown in Vokrouhlický et al. (2003), spin-orbit resonances can have a major effect on obliquity evolution. All of these factors produce complicated feedbacks that can modify asteroid drift rates and rotation rate changes. Because YORP is sensitive to the

size, shape, material properties, and asteroid location, this effect will also vary from object to object. This means that despite progress toward computing a chronology of asteroid families (e.g., Carruba et al. 2003, Vokrouhlický et al. 2005a), obtaining high-precision solutions will take considerable effort. Future work on the YORP effect will also have to account for thermal relaxation and more refined thermophysics (e.g., Spitale & Greenberg 2001, 2002).

We also need to better understand the endstates of YORP evolution. For example, if YORP spins up an asteroid fast enough, it should undergo fission and possibly produce an asteroid satellite. On the other hand, YORP may also limit the dynamical lifetime of synchronous rotating binaries (Ćuk & Burns 2005). For asteroids spun down by YORP, some may enter into a chaotic "tumbling" rotation state similar to that observed for Toutatis and other asteroids (e.g., Pravec & Harris 2002). How asteroids reemerge from a tumbling state has yet to be studied in detail, although preliminary work indicates that the threshold where tumbling takes place depends sensitively on the dissipation rate of internal energy in a given body. Finally, we have yet to compute accurate YORP torques for meter-sized bodies; doing so may require more sophisticated heat transfer models than have been used to date.

These problems, which are critical to our understanding of small-body evolution, will keep the study of nongravitational effects on asteroids and meteoroids an active field of research for the foreseeable future.

ACKNOWLEDGMENTS

This review has benefited from past work and discussions with Míra Brož, Dan Durda, Hal Levison, Alessandro Morbidelli, and Bill Ward. W.F. Bottke and D. Nesvorný gratefully acknowledge support from NASA's Planetary Geology and Geophysics program. The work of D. Vokrouhlický was supported by the Grant Agency of the Czech Republic.

LITERATURE CITED

Alfonso GB, Gomes RS, Florczak MA. 1995. Asteroid fragments in Earth-crossing orbits. *Planet. Space Sci.* 43:787–95

Beekman G. 2005. I.O. Yarkovsky and the discovery of 'his' effect. *J. Hist. Astron.* In press

Benz W, Asphaug E. 1999. Catastrophic disruptions revisited. *Icarus* 142:5–20

Binzel RP, Farinella P, Zappalà V, Cellino A. 1989. Asteroid rotation rates - Distributions and statistics. In *Asteroids II*, ed. RP Binzel, T Gehrels, MS Matthews, pp. 416–41. Tucson: Univ. Ariz. Press

Binzel RP, Rivkin AS, Stuart JS, Harris AW, Bus SJ, Burbine TH. 2004. Observed spectral properties of near-Earth objects: results for population distribution, source regions, and spaceweathering processes. *Icarus* 170:259–94

Bottke WF, Cellino A, Paolicchi P, Binzel RP, eds. 2002. *Asteroids III.* Tucson: Univ. Ariz. Press

Bottke WF, Durda DD, Nesvorný D, Jedicke R, Morbidelli A, et al. 2005a. The fossilized size distribution of the main asteroid belt. *Icarus* 175:111–40

Bottke WF, Durda DD, Nesvorný D, Jedicke R, Morbidelli A, et al. 2005b. Linking the collisional evolution of the main belt to its dynamical excitation and depletion. *Icarus* 179:63–94

Bottke WF, Durda DD, Nesvorný D, Jedicke R, Morbidelli A, et al. 2005c. The origin and evolution of stony meteorites. In *Dynamics of Populations of Planetary Systems*, ed. Z Knežević, A Milani, pp. 357–76. Cambridge: Cambridge Univ. Press

Bottke WF, Jedicke R, Morbidelli A, Petit JM, Gladman B. 2000a. Understanding the distribution of near-Earth asteroids. *Science* 288:2190–94

Bottke WF, Morbidelli A, Jedicke R, Petit JM, Levison HF, et al. 2002b. Debiased orbital and absolute magnitude distribution of the near-Earth objects. *Icarus* 156:399–433

Bottke WF, Nolan MC, Greenberg R, Kolvoord RA. 1994. Velocity distributions among colliding asteroids. *Icarus* 107:255–68

Bottke WF, Rubincam DP, Burns JA. 2000b. Dynamical evolution of main belt meteoroids: Numerical simulations incorporating planetary perturbations and Yarkovsky thermal forces. *Icarus* 145:301–31

Bottke WF, Vokrouhlický D, Brož M, Nesvorný D, Morbidelli A. 2001. Dynamical spreading of asteroid families by the Yarkovsky effect. *Science* 294:1693–96

Bottke WF, Vokrouhlický D, Rubincam D, Brož B. 2002a. Dynamical evolution of asteroids and meteoroids using the Yarkovsky Effect. See Bottke et al. 2002, pp. 395–408

Brož M, Vokrouhlický D, Roig F, Nesvorný D, Bottke WF, Morbidelli A. 2005. Yarkovsky origin of the unstable asteroids in the 2/1 mean motion resonance with Jupiter. *MNRAS* 359:1437–55

Burns JA, Lamy PL, Soter S. 1979. Radiation forces on small particles in the solar system. *Icarus* 40:1–48

Čapek D, Vokrouhlický D. 2004. The YORP effect with finite thermal conductivity. *Icarus* 172:526–36

Carruba V, Burns JA, Bottke WF, Nesvorný D. 2003. Orbital evolution of the Gefion and Adeona asteroid families: close encounters with massive asteroids and the Yarkovsky effect. *Icarus* 162:308–27

Cellino A, Bus SJ, Doressoundiram A, Lazzaro D. 2002. Spectroscopic properties of asteroid families. See Bottke et al. 2002, pp. 633–43

Cellino A, Michel P, Tanga P, Zappalà V, Paolicchi P, Dell'Oro A. 1999. The velocity-size relationship for members of asteroid families and implications for the physics of catastrophic collisions. *Icarus* 141:79–95

Chesley SR, Ostro SJ, Vokrouhlický D, Čapek D, Giorgini JD, et al. 2003. Direct detection of the Yarkovsky effect by radar ranging to asteroid 6489 Golevka. *Science* 302:1739–42

Ćuk M, Burns JA. 2005. Effects of thermal radiation on the dynamics of binary NEAs. *Icarus* 176:418–31

Davis DR, Weidenschilling SJ, Farinella P, Paolicchi P, Binzel RP. 1989. Asteroid collisional history - Effects on sizes and spins. See Binzel et al. 1989, pp. 805–26

Dell'Oro A, Bigongiari G, Paolicchi P, Cellino A. 2004. Asteroid families: evidence of ageing of the proper elements. *Icarus* 169:341–56
Dobrovolskis AR. 1996. Inertia of any polyhedron. *Icarus* 124:698–704
Dohnanyi JS. 1978. Particle dynamics. In *Cosmic Dust*, ed. JAM McDonnell, pp. 527–605. Chichester, UK: Wiley-Intersci.
Eugster O. 2003. Cosmic-ray exposure ages of meteorites and lunar rocks and their significance. *Chem. Erde* 63:3–30
Farinella P, Froeschlé Ch, Froeschlé C, Gonczi R, Hahn G, et al. 1994. Asteroids falling onto the Sun. *Nature* 371:315–16
Farinella P, Gonczi R, Froeschlé C, Froeschlé Ch. 1993. The injection of asteroid fragments into resonances. *Icarus* 101:174–87
Farinella P, Vokrouhlický D. 1999. Semimajor axis mobility of asteroidal fragments. *Science* 283:1507–10
Farinella P, Vokrouhlický D, Hartmann WK. 1998. Meteorite delivery via Yarkovsky orbital drift. *Icarus* 132:378–87
Gladman BJ, Migliorini F, Morbidelli A, Zappalà V, Michel P, et al. 1997. Dynamical lifetimes of objects injected into asteroid belt resonances. *Science* 277:197–201
Grieve RAF, Shoemaker EM. 1994. The record of past impacts on Earth. In *Hazards Due to Comets and Asteroids*, ed. T Gehrels, MS Matthews, pp. 417–62. Tucson: Univ. Ariz. Press
Hartmann WK, Farinella P, Vokrouhlický D, Weidenschilling SJ, Morbidelli A, et al. 1999. Reviewing the Yarkovsky effect: New light on the delivery of stone and iron meteorites from the asteroid belt. *Meteorit. Planet. Sci.* 34:161–67
Holsapple KA. 2005. Asteroid spin data: No evidence of rubble-pile structures. *Lunar Planet. Sci.* 36:2329
Hudson RS, Ostro SJ, Jurgens RF, Rosema KD, Giorgini JD, et al. 2000. Radar observations and physical modeling of asteroid 6489 Golevka. *Icarus* 148:37–51
Katasev LA, Kulikova NV. 1980. Physical and mathematical modeling of the formation and evolution of meteor streams II. *Astron. Vestn.* 14:225–29
Knežević Z, Milani A, Farinella P. 1997. The dangerous border of the 5:2 mean motion resonance. *Planet. Space Sci.* 45:1581–85
Knežević Z, Lemaître A, Milani A. 2002. The determination of asteroid proper elements. See Bottke et al. 2002, pp. 603–12
La Spina A, Paolicchi P, Kryszczińska A, Pravec P. 2004. Retrograde spins of near-Earth asteroids from the Yarkovsky effect. *Nature* 428:400–1
McEwen AS, Moore JM, Shoemaker EM. 1997. The Phanerozoic impact cratering rate: Evidence from the farside of the Moon. *J. Geophys. Res.* 102:9231–42
McEwen AS, Preblich BS, Turtle EP, Artemieva NA, Golombek MP, et al. 2005. The rayed crater Zunil and interpretations of small impact craters on Mars. *Icarus* 176:351–81
Michel P, Benz W, Tanga P, Richardson D. 2001. Collisions and gravitational reaccumulation: A recipe for forming asteroid families and satellites. *Science* 294:1696–700
Michel P, Migliorini F, Morbidelli A, Zappalà V. 2000. The population of Mars-crossers: Classification and dynamical evolution. *Icarus* 145:332–47

Migliorini F, Michel P, Morbidelli A, Nesvorný D, Zappalà V. 1998. Origin of Earth-crossing asteroids: a quantitative simulation. *Science* 281:2022–24
Migliorini F, Morbidelli A, Zappalà V, Gladman BJ, Bailey ME, Cellino A. 1997. Vesta fragments from v6 and 3:1 resonances: implications for V-type NEAs and HED meteorites. *Meteorit. Planet. Sci.* 32:903–16
Milani A, Farinella P. 1995. An asteroid on the brink. *Icarus* 115:209–12
Milani A, Knežević Z. 1994. Asteroid proper elements and the dynamical structure of the asteroid main belt. *Icarus* 107:219–54
Morbidelli A, Gladman B. 1998. Orbital and temporal distributions of meteorites originating in the asteroid belt. *Meteorit. Planet. Sci.* 33:999–1016
Morbidelli A, Nesvorný D. 1999. Numerous weak resonances drive asteroids toward terrestrial planets orbits. *Icarus* 139:295–308
Morbidelli A, Vokrouhlický D. 2003. The Yarkovsky-driven origin of near-Earth asteroids. *Icarus* 163:120–34
Muinonen K. 1998. Introducing the Gaussian shape hypothesis for asteroids and comets. *Astron. Astrophys.* 332:1087–98
Neiman VB, Romanov EM, Chernov VM. 1965. Ivan Osipovich Yarkovsky. *Earth Univ.* 4:63-64 (Russ. mag.)
Nesvorný D, Bottke WF. 2004. Detection of the Yarkovsky effect for main-belt asteroids. *Icarus* 170:324–42
Nesvorný D, Bottke WF, Dones L, Levison HF. 2002b. The recent breakup of an asteroid in the main-belt region. *Nature* 417:720–22
Nesvorný D, Bottke WF, Dones L, Levison HF. 2003. Recent origin of the Solar System dust bands. *Astrophys. J.* 591:486–97
Nesvorný D, Morbidelli A, Vokrouhlický D, Bottke WF, Brož M. 2002a. The Flora family: A case of the dynamically dispersed collisional swarm? *Icarus* 157:155–72
Nesvorný D, Vokrouhlický D, Bottke WF, Sykes M. 2005. Physical properties of asteroid dust bands and their sources. *Icarus*. In press
O'Keefe JA. 1976. *Tektites and Their Origin. Developments in Petrology, No. 4*. Amsterdam: Elsevier
Olsson-Steel D. 1986. The origin of the sporadic meteoroid component. *MNRAS* 219:47–73
Olsson-Steel D. 1987. The dispersal of the Geminid meteoroid stream by radiative effects. *MNRAS* 226:1–17
Öpik EJ. 1951. Collision probabilities with the planets and the distribution of interplanetary matter. *Proc. R. Irish Acad.* 54A:165–99
Öpik EJ. 1976. *Interplanetary Encounters.* Elsevier: New York
Paddack SJ. 1969. Rotational bursting of small celestial bodies: effects of radiation pressure. *J. Geophys. Res.* 74:4379–81
Paddack SJ. 1973. *Rotational bursting of small particles.* PhD thesis. Catholic Univ. Washington, DC
Paddack SJ, Rhee JW. 1975. Rotational bursting of interplanetary dust particles. *Geophys. Res. Lett.* 2:365–67
Peterson C. 1976. A source mechanism for meteorites controlled by the Yarkovsky effect. *Icarus* 29:91–111

Pravec P, Harris AW. 2000. Fast and slow rotation of asteroids. *Icarus* 148:12–20
Pravec P, Harris AW, Michalowski T. 2002. Asteroid rotations. See Bottke et al. 2002, pp. 113–22
Radzievskii VV. 1952. About the influence of the anisotropically reemited solar radiation on the orbits of asteroids and meteoroids. *Astron. Zh.* 29:162–70
Radzievskii VV. 1954. A mechanism for the disintegration of asteroids and meteorites. *Dokl. Akad. Nauk SSSR* 97:49–52
Richardson DC, Leinhardt ZM, Melosh HJ, Bottke WF, Asphaug E. 2002. Gravitational aggregates: Evidence and evolution. See Bottke et al. 2002, pp. 501–15
Rubincam DP. 1987. LAGEOS orbit decay due to infrared radiation from earth. *J. Geophys. Res.* 92:1287–94
Rubincam DP. 1988. Yarkovsky thermal drag on LAGEOS. *J. Geophys. Res.* 93:13805–10
Rubincam DP. 1990. Drag on the LAGEOS satellite. *J. Geophys. Res.* 95:4881–86
Rubincam DP. 1995. Asteroid orbit evolution due to thermal drag. *J. Geophys. Res.* 100:1585–94
Rubincam DP. 1998. Yarkovsky thermal drag on small asteroids and Mars-Earth delivery. *J. Geophys. Res.* 103:1725–32
Rubincam DP. 2000. Radiative spin-up and spin-down of small asteroids. *Icarus* 148:2–11
Rubincam DP, Rowlands DD, Ray RD. 2002. Is asteroid 951 Gaspra in a resonant obliquity state with its spin increasing due to YORP? *J. Geophys. Res.* 107(E9):5065
Simonelli DP, Thomas PC, Carcich BT, Veverka J. 1993. The generation and use of numerical shape models for irregular Solar System objects. *Icarus* 103:49–61
Skoglöv E. 1999. Spin vector evolution for inner solar system asteroids. *Planet. Space Sci.* 47:11–22
Slabinski VJ. 1977. Solar radiation torques on meteoroids: complications for the Yarkovsky effect from spin axis precession. *BAAS* 9:438
Slivan SM. 2002. Spin vector alignment of Koronis family asteroids. *Nature* 419:49–51
Slivan SM, Binzel RP, Crespo da Silva LD, Kaasalainen M, Lyndaker MM, Krčo M. 2003. Spin vectors in the Koronis family: comprehensive results from two independent analyses of 213 rotation lightcurves. *Icarus* 162:285–307
Spitale J, Greenberg R. 2001. Numerical evaluation of the general Yarkovsky effect: Effects on semimajor axis. *Icarus* 149:222–34
Spitale J, Greenberg R. 2002. Numerical evaluation of the general Yarkovsky effect: Effects on eccentricity and longitude of periapse. *Icarus* 156:211–22
Stuart JS, Binzel RP. 2004. Bias-corrected population, size distribution, and impact hazard for the near-Earth objects. *Icarus* 170:295–311
Tanga P, Cellino A, Michel P, Zappalà V, Paolicchi P, Dell'Oro A. 1999. On the size distribution of asteroid families: The role of geometry. *Icarus* 141:65–78
Tsiganis K, Varvoglis H, Morbidelli A. 2003. Short-lived asteroids in the 7/3 Kirkwood gap and their relationship to the Koronis and Eos families. *Icarus* 166:131–40

Vokrouhlický D. 1998a. Diurnal Yarkovsky effect as a source of mobility of meter-sized asteroidal fragments. I. Linear theory. *Astron. Astrophys.* 335:1093–100
Vokrouhlický D. 1998b. Diurnal Yarkovsky effect as a source of mobility of meter-sized asteroidal fragments. II. Non-sphericity effects. *Astron. Astrophys.* 338:353–63
Vokrouhlický D. 1999. A complete linear model for the Yarkovsky thermal force on spherical asteroid fragments. *Astron. Astrophys.* 344:362–66
Vokrouhlický D. 2001. The Yarkovsky effect in the dynamics of the Solar System. In *The Restless Universe: Applications of Gravitational N-Body Dynamics to Planetary, Stellar and Galactic Systems*, ed. BA Steves, AJ Maciejewski, pp. 53–78. Bristol, UK: Inst. Phys.
Vokrouhlický D, Bottke WF. 2001. The Yarkovsky thermal force on small asteroids and their fragments. Choosing the right albedo. *Astron. Astrophys.* 371:350–53
Vokrouhlický D, Brož M, Bottke WF, Nesvorný D, Morbidelli A. 2005d. Yarkovsky/YORP chronology of young asteroid families. *Icarus*. In press
Vokrouhlický D, Brož M, Farinella P, Knežević Z. 2001b. Yarkovsky-driven leakage of Koronis family members. *Icarus* 150:78–93
Vokrouhlický D, Brož M, Morbidelli A, Bottke WF, Nesvorný D, et al. 2005c. The evolution of the Eos family by Yarkovsky evolution. *Icarus*. In press
Vokrouhlický D, Čapek D. 2002. YORP-induced long-term evolution of the spin state of small asteroids and meteoroids. I. Rubincam's approximation. *Icarus* 159:449–67
Vokrouhlický D, Čapek D, Chesley SR, Ostro SJ. 2005a. Yarkovsky detection opportunities. I. Solitary asteroids. *Icarus* 173:166–84
Vokrouhlický D, Čapek D, Chesley SR, Ostro SJ. 2005b. Yarkovsky detection opportunities. I. Binary asteroids. *Icarus* 179:128–38
Vokrouhlický D, Čapek D, Kaasalainen M, Ostro SJ. 2004. Detectability of YORP rotational slowing of asteroid 25143 Itokawa. *Astron. Astrophys.* 414:L21–24
Vokrouhlický D, Chesley SR, Milani A. 2001a. On the observability of radiation forces acting on near-Earth asteroids. *Celest. Mech. Dyn. Astron.* 81:149–65
Vokrouhlický D, Farinella P. 1998. The Yarkovsky seasonal effect on asteroidal fragments: A nonlinearized theory for the plane-parallel case. *Astron. J.* 116:2032–41
Vokrouhlický D, Farinella P. 1999. The Yarkovsky seasonal effect on asteroidal fragments: A nonlinearized theory for spherical bodies. *Astron. J.* 118:3049–60
Vokrouhlický D, Farinella P. 2000. Efficient delivery of meteorites to the Earth from a wide range of asteroid parent bodies. *Nature* 407:606–8
Vokrouhlický D, Milani A, Chesley SR. 2000. Yarkovsky effect on small near-Earth asteroids: Mathematical formulation and examples. *Icarus* 148:118–38
Vokrouhlický D, Nesvorný D, Bottke WF. 2003. Thermal torques produce spin vector alignments among Koronis family asteroids. *Nature* 425:147–52
Wetherill GW. 1979. Steady state populations of Apollo-Amor objects. *Icarus* 37:96–112
Whipple FL. 1950. A comet model. I. The acceleration of Comet Encke. *Astrophys. J.* 111:375–94

Wisdom J. 1983. Chaotic behavior and the origin of the 3/1 Kirkwood gap. *Icarus* 56:51–74

Zappalà V, Bendjoya P, Cellino A, Di Martino A, Doressoundiram A, et al. 2000. Fugitives from the Eos family: First spectroscopic confirmation. *Icarus* 145:4–11

Zappalà V, Cellino A, Dell'Oro A. 2002. A search for the collisional parent bodies of large NEAs. *Icarus* 157:280–96

Zappalà V, Cellino A, Dell'Oro A, Migliorini F, Paolicchi P. 1996. Reconstructing the original ejection velocity fields of asteroid families. *Icarus* 124:156–80

Annual Review of Earth and Planetary Sciences

Volume 34, 2006

Contents

INDEXES

ERRATA

An online log of corrections to *Annual Review of Earth and Planetary Sciences* chapters may be found at http://earth.annualreviews.org